AD-A128 819 DEMONSTRATION OF THE ELECTRIC CURRENT PERTURBATION TECHNIQUE FOR FATIGUE..(U) SOUTHWEST RESEARCH INST SAN ANTONIO TX G L BURKHARDT ET AL. NOV 79 1/1

UNCLASSIFIED SWRI-15-5607-802 DLA900-79-C-1266 F/G 14/2 NL

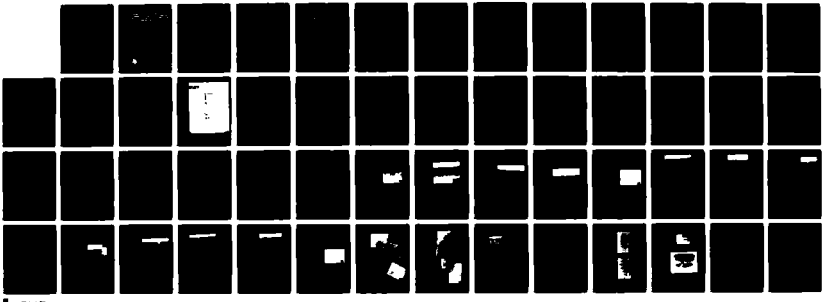

END

DATE FILMED

6-83

DTIC

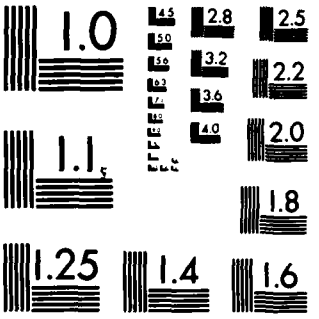

DEMONSTRATION OF THE ELECTRIC CURRENT PERTURBATION TECHNIQUE FOR FATIGUE CRACK CHARACTERIZATION IN TF-33 TURBINE DISK TIEBOLT HOLES

FINAL REPORT

under

Contract Nos. DLA900-79-C-1266 and F41608-79-D-A011-0011
SwRI Projects 15-5607-802 and 15-5459-024

for

Air Force Materials Laboratory/LLP
Wright Patterson AFB, OH

November 1979

SOUTHWEST RESEARCH INSTITUTE
SAN ANTONIO HOUSTON

REPORT DOCUMENTATION PAGE

READ INSTRUCTIONS BEFORE COMPLETING FORM

1. REPORT NUMBER	2. GOVT ACCESSION NO. AD-A128 814
3. RECIPIENT'S CATALOG NUMBER	
4. TITLE *(and Subtitle)*	5. TYPE OF REPORT & PERIOD COVERED
Demonstration of the Electric Current Perturbation Technique for Fatigue Crack Characterization in TF-33 Turbine Disk Tiebolt Holes	Final Report
	6. PERFORMING ORG. REPORT NUMBER SwRI 15-5607-802
7. AUTHOR(s)	8. CONTRACT OR GRANT NUMBER(s)
Gary L. Burkhardt, Robert E. Beissner, Cecil M. Teller, John R. Barton	DLA900-79-C-1266
9. PERFORMING ORGANIZATION NAME AND ADDRESSES Southwest Research Institute P.O. Drawer 28510 San Antonio, TX 78284	10. PROGRAM ELEMENT, PROJECT, TASK AREA & WORK UNIT NUMBERS
11. CONTROLLING OFFICE NAME AND ADDRESS Air Force Materials Laboratory/LLP Wright Patterson AFB, OH	12. REPORT DATE November 1979 13. NUMBER OF PAGES 47
14. MONITORING AGENCY NAME & ADDRESS *(if different from Controlling Office)*	15. SECURITY CLASS. *(of this report)* UNCLASSIFIED 15a. DECLASSIFICATION/DOWNGRADING SCHEDULE

16. DISTRIBUTION STATEMENT *(of this Report)*

Approved for public release; distribution unlimited.

17. DISTRIBUTION STATEMENT *(of the abstract entered in Block 20, if different from Report)*

18. SUPPLEMENTARY NOTES

19. KEY WORDS *(Continue on reverse side if necessary and identify by block number)*

turbine disks
fatigue cracks
electric current perturbation
nondestructive testing

20. ABSTRACT *(Continue on reverse side if necessary and identify by block number)*

The Electric Current Perturbation (ECP) technique was evaluated to demonstrate its capability to detect and characterize low-cycle fatigue cracks in tiebolt holes of TF-33, third-stage turbine disks. Examinations were performed on one hundred tiebolt holes in ten scrap disks. Signatures were correlated with twelve cracks which were metallurgically examined and sectioned to determine crack size, shape and orientation. Correlation of ECP signatures with the metallurgical results confirmed detection in one case of a very small and

20. (Cont'd)

relatively isolated crack of approximately 0.30 mm (12 mils) surface length by 0.14 mm (5.4 mils) deep. Smaller cracks were also detected; however, their signals were complicated by influences from adjacent cracks. Calculations indicate that the ECP method is capable of detecting cracks approximately 0.25 mm (10 mils) long by 0.08 mm (3 mils) deep at a signal-to-background ratio of approximately two with the present probe design. An overall appraisal indicates that the ECP method offers high sensitivity even to very small fatigue cracks; the potential to discriminate between single and multiple cracks; and the potential to obtain crack characterization parameters.

SOUTHWEST RESEARCH INSTITUTE
Post Office Drawer 28510, 6220 Culebra Road
San Antonio, Texas 78284

DEMONSTRATION OF THE ELECTRIC CURRENT PERTURBATION TECHNIQUE FOR FATIGUE CRACK CHARACTERIZATION IN TF-33 TURBINE DISK TIEBOLT HOLES

by

Gary L. Burkhardt
Cecil M. Teller
Robert E. Biessner
John R. Barton

FINAL REPORT

under

Contract Nos. DLA900-79-C-1266 and F41608-79-D-A011-~~0011~~
SwRI Projects 15-5607-802 and 15-5459-024

for

Air Force Materials Laboratory/LLP
Wright Patterson AFB, OH

November 1979

Approved:

John R. Barton

John R. Barton, Vice President
Instrumentation Research Division

ABSTRACT

The Electric Current Perturbation (ECP) technique was evaluated to demonstrate its capability to detect and characterize low-cycle fatigue cracks in tiebolt holes of TF-33, third-stage turbine disks. Examinations were performed on one hundred tiebolt holes in ten scrap disks. Signatures were correlated with twelve cracks which were metallurgically examined and sectioned to determine crack size, shape and orientation. Correlation of ECP signatures with the metallurgical results confirmed detection in one case of a very small and relatively isolated crack of approximately 0.30 mm (12 mils) surface length by 0.14 mm (5.4 mils) deep. Smaller cracks were also detected; however, their signals were complicated by influences from adjacent cracks. Calculations indicate that the ECP method is capable of detecting cracks approximately 0.25 mm (10 mils) long by 0.08 mm (3 mils) deep at a signal-to-background ratio of approximately two with the present probe design. An overall appraisal indicates that the ECP method offers high sensitivity even to very small fatigue cracks; the potential to discriminate between single and multiple cracks; and the potential to obtain crack characterization parameters.

TABLE OF CONTENTS

LIST OF ILLUSTRATIONS

LIST OF ILLUSTRATIONS (continued)

I. INTRODUCTION

A. Background

The nondestructive detection and sizing of (1) tightly closed low cycle fatigue cracks in gas turbine engine disks and (2) fatigue cracks emanating from fastener holes in structural elements of aircraft are two of the most pressing problems confronting the Air Force. A number of nondestructive methods are being used, refined, developed or considered as long-term solutions for those two critical problems. Included are fluorescent penetrant, eddy current, ultrasonics, acoustic emission and laser surface scan.

Another method, electric current perturbation (ECP), which has been pioneered and under investigation by Southwest Research Institute for more than a decade, is also a candidate with unique advantages. In this method an electric current flow is established in the region of the component or structure to be examined and conduction anomalies perturb the current flow. This perturbed current flow is sensed by a non-contacting magnetometer that is sensitive to the magnetic field associated with the current perturbation. The method has been used in exploratory investigations of materials such as brass, aluminum, titanium, Zircaloy, and superalloys and has been demonstrated to have the capability for detecting small flaws, fatigue cracks and other conduction anomalies, both surface and subsurface.

In 1977, Southwest Research Institute initiated a project under its IR&D program to conduct an extensive investigation of the ECP method. Program elements included: theory, analytical modeling, experimental data acquisition and analyses, and rudimentary imaging displays. In addition to other objectives the investigation would provide a preliminary assessment of the potential effectiveness of the method applied to the two previously mentioned critical Air Force problems. Mr. D. M. Forney (AFML/LLP) was appraised of this activity by SwRI representatives and indicated that if the NDE results showed sufficient justification he would attempt to obtain Air Force funding for further work. It was considered essential that actual service-fatigued components be available for elements of the program and Dr. W. H. Reimann (AFML/LLN) assisted in obtaining TF-33 retired disks from OCALC and also several small bolt-hole specimens with known fatigue cracks excised from disks. Mr. B. W. Boisvert (SAALC/MMETP) assisted in providing sections of aircraft wings with fastener fatigue cracked regions for evaluation on the program. Results from the early phases of this SwRI funded effort were informally reviewed with Forney and Reimann and subsequently a limited effort, including metallurgical verification, was proposed to Forney. Authorization to initiate the effort was received 28 March 1979 and this report summarizes results of the project. Results are briefly summarized below and a description of the method, apparatus, specimens, data acquisition and correlation of metallurgical sectioning results are detailed in subsequent sections.

B. Summary

The ECP technique was evaluated in this project to demonstrate the capability to detect and characterize low cycle fatigue (LCF) cracks in tiebolt holes of TF-33, third stage turbine disks, fabricated from wrought Incoloy 901. ECP examinations were performed on ten tiebolt

holes in each of ten scrap TF-33 disks obtained from OCALC, Tinker AFB, OK. ECP data were obtained as the probe was scanned circumferentially in each hole at increments along the axial length of the hole. Based on analysis of the data from all 100 holes, four were selected which had signatures with signal-to-background ratios of approximately two or greater. Specimens containing each of these four holes (bore side) were excised from the disk so that the samples could be examined metallurgically. Both optical and scanning electron microscope (SEM) examinations of the specimen surfaces were made for observations of fatigue cracks. Selected cracks were then sectioned metallurgically at various increments along the crack length to determine the subsurface crack geometry and obtain depth information. These data were then correlated with the ECP signal obtained from each region.

Data from the four holes selected for sectioning showed that each specimen contained several small fatigue cracks. Correlation of ECP signatures with the metallurgical results confirmed detection in one case of a very small, relatively isolated crack of approximately 0.30 mm (12 mils) surface length by 0.14 mm (5.4 mils) deep; correlation of other cracks with ECP signatures was also confirmed. An overall appraisal indicates that the ECP method offers high sensitivity even to very small fatigue cracks; the potential to discriminate between single and multiple cracks; and the potential to obtain crack characterization parameters.

II. DESCRIPTION OF THE ELECTRIC CURRENT PERTURBATION METHOD

In electric current perturbation inspection a direct current or an alternating current is established in the material to be inspected by either direct contact or induction. Current perturbations caused by nonconducting interfaces and areas of varying conduction such as fatigue cracks are then measured to infer the quality of the item being inspected. Since it is difficult to determine the current perturbations by potential measurements using contacting electrodes, an alternate detection method is employed. This method consists of measuring the magnetic field components associated with the components of the current perturbation. The magnetic field perturbations are detected with a small differential inductive pickup coil (passive) placed near the surface of the material. The probe can be made noncontacting by using air liftoff.

To illustrate the concepts involved in such a method, it is instructive to examine the current-magnetic field distribution associated th a current carrying slotted plate. Figure 1 is a sketch depicting h a plate. The dashed line in 1a and 1b views represents a slot whi has been cut partially through the thin plate. If the plate had n been slotted, the current distribution within the plate would be u orm. However, as represented in this figure, the slot affects the unifc current distribution in two ways. First, the current tends to det around the slot ends as shown in Figure 1b; second, the current tends to detour over the slot as in Figure 1c. These current detours result in changes or perturbations of the external magnetic flux. Specifically, the current detour around the end of the slot deviates the flux from its normal direction which is parallel to the slots (see Figure 1b). Also, the current detour over the slot results in an increased current density in the vicinity of the slot and will consequently increase the magnetic flux magnitude at the plate surface.

Consider the problem of measuring the flux perturbations described. The major component of the magnetic flux has a direction at the plate surface which is tangential to this surface, perpendicular to the undistorted current flow and parallel to the slot. For shallow slots, the flux perturbation in the direction of the main field will be small and will be difficult to measure when superimposed on the main magnetic field. Fortunately, there are flux perturbations in two other directions perpendicular to the main field direction which can be measured without being obscured by the main field. These directions are indicated by V and T in Figure 1.

Figure 2 is a schematic representation of the current flow, the slot and the magnetic field distribution. Three different scan paths are shown in this illustration; path 1 and path 2 are parallel to the slot while path 3 is perpendicular to the slot. The shapes of the tangential component ϕp of the magnetic field perturbation encountered along scan path 1 and 2 are shown as signal (1) and signal (2). The vertical component of the magnetic field perturbation encountered along scan path 3 is shown as signal (3). The shapes of perturbation along scan path 1 and 2 are of particular interest, since they demonstrate a reversal of polarity near the ends of the slot as well as an

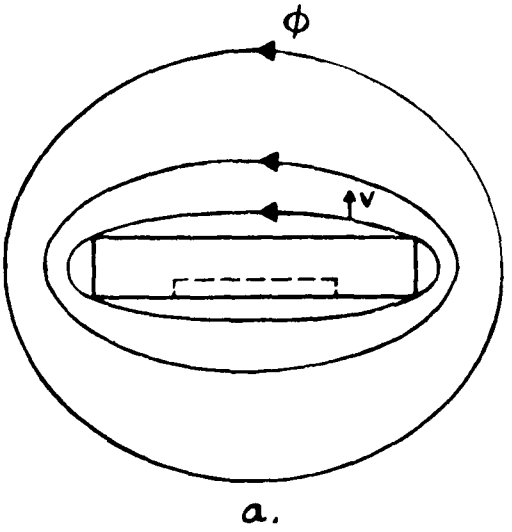

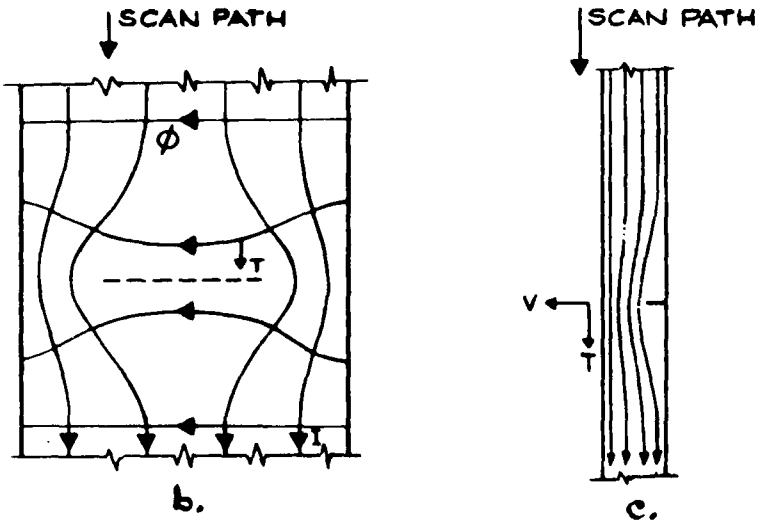

FIGURE 1. PICTORIAL FIELD PLOT OF A CURRENT CARRYING SLOTTED PLATE

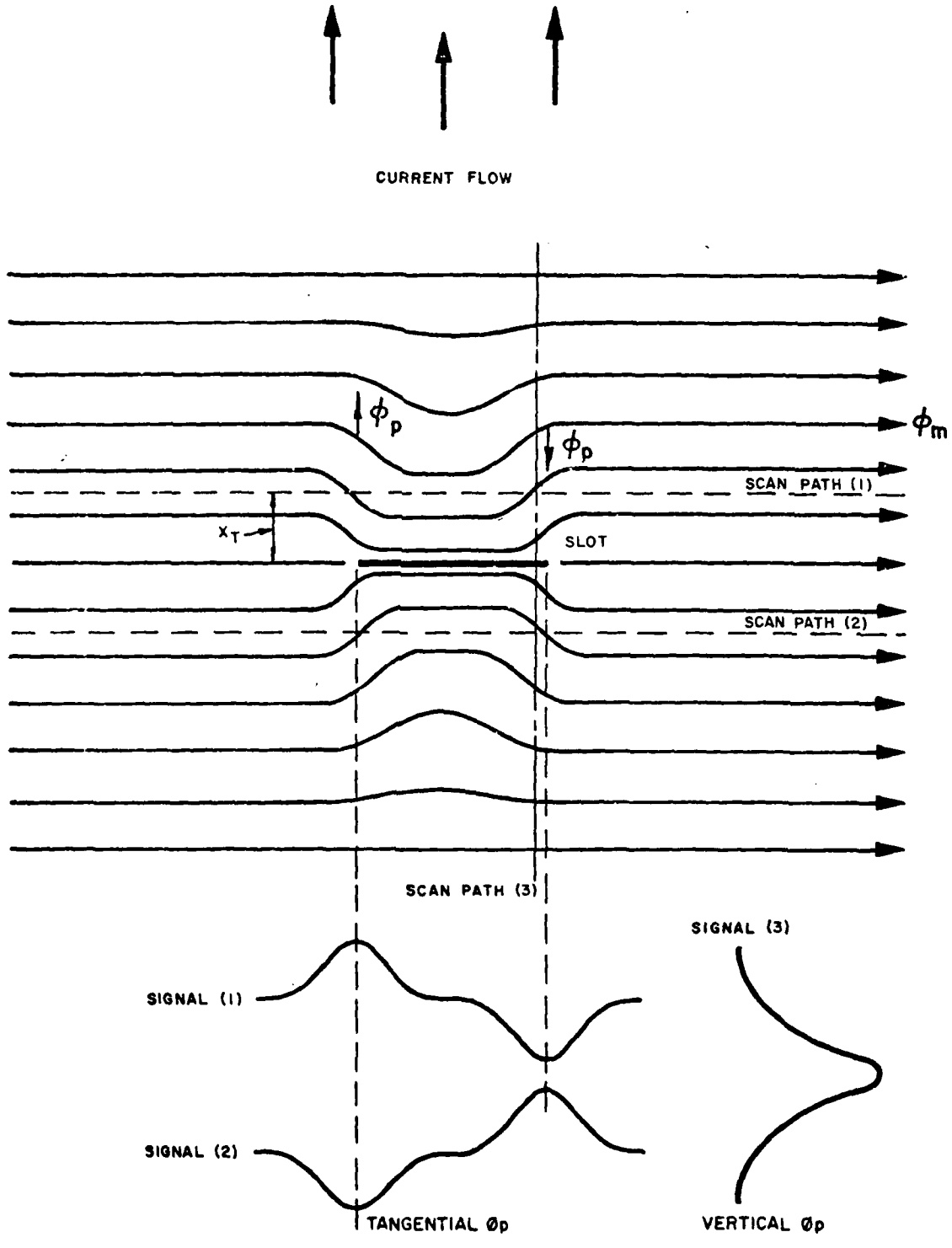

FIGURE 2. MAGNETIC FIELD DISTRIBUTION ABOUT A SLOT AND SIGNALS PRODUCED BY TANGENTIAL AND VERTICAL COMPONENTS

opposite polarity associated with scans made on opposite sides of the slot. Such characteristics are useful in identifying the location and shapes of signal sources.

III. EXPERIMENTAL ARRANGEMENT

A. Setup and Procedure

The rudimentary scanning apparatus used in the investigation is shown positioned on a TF-33 disk in Figure 3. The ECP probe utilizes a noncontacting induction method for establishing current flow in the tie-bolt hole. The scanning system incorporates a motor for driving the probe in a circumferential direction and a manual positioning arrangement to allow precise axial probe positioning; a shaft angle encoder supplies pulses to indicate probe position on each scan. With this scanner, the operator positions the probe axially and initiates the start of each scan. Upon completion of a series of scans on one hole, the probe was removed from the hole and the entire scanning assembly was manually positioned in the next hole.

ECP records were acquired on tiebolt holes in ten scrap TF-33 jet engine third stage turbine disks. Ten holes in each disk (total of 100) were inspected using a circumferential scan procedure in which the first scan was located at a distance of 0.64 mm (25 mils) from the top surface of the disk (hole) and successive scans were located at 0.64 mm (25 mil) increments for a total of 32 scans per hole. Data were recorded on a 2-channel strip-chart recorder.

ECP signals from most holes were very large, ranging up to 38 V in amplitude. Since one of the objectives was to assess applicability of the ECP method for detecting and sizing small cracks, a review of records was made to select signature regions with an S/N ratio of 2 (based on material background noise) or 120 mV. These regions would be candidates for metallurgical sectioning. Inasmuch as the disks examined had been retired from service because of large fatigue cracks or a high number of in-service cycle-hours, the selection of holes with ECP signals of the desired amplitude was very limited and no holes containing a single isolated signal were found. Four holes with signals in the desired range were found, however, and these holes, plus one additional hole into which air-abrasive slots had been introduced as targets of known size, were scanned again at 0.32 mm (12.5 mil) increments between scans for a total of 64 scans per hole. These data were recorded both on strip-chart and on analog magnetic tape. Table I lists serial numbers of all ten disks examined, the number of in-service cycles for each disk, and the total number of in-service hours for five disks. Also shown are the holes which were selected for magnetic tape data and strip-chart data at 0.32 mm (12.5 mil) increments. The four selected holes were then sectioned to determine crack geometry.

B. Data Format

Figure 4 shows the scan geometry used in the acquisition of ECP data. The side of the disk designated as "top" is the one containing disk serial numbers, and the scans were made in a clockwise direction from the starting point shown in the figure. A typical ECP signature is shown in

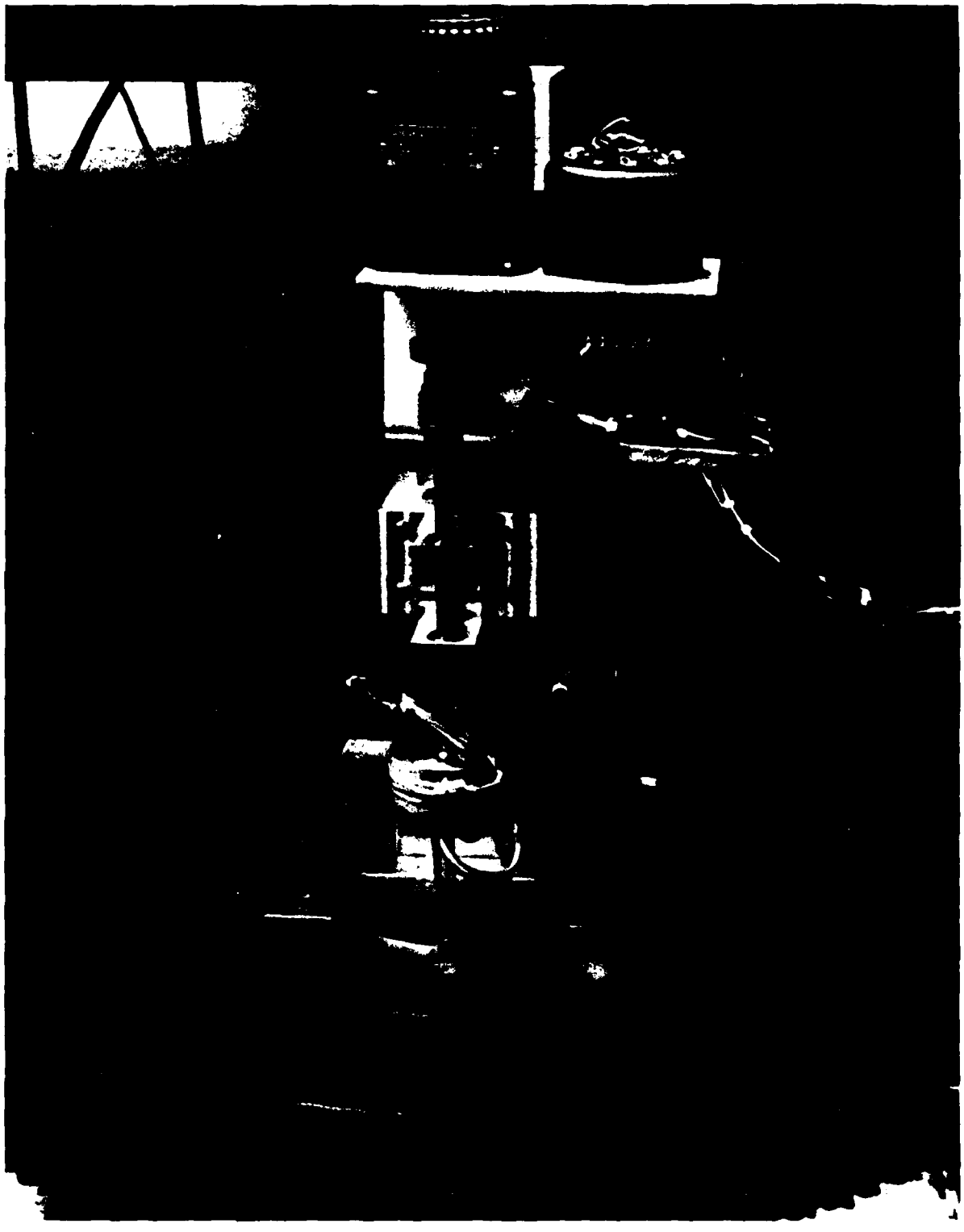

5517

FIGURE 3. RUDIMENTARY ECP SCANNING SYSTEM

TABLE I

TURBINE DISKS INSPECTED (TF-33, THIRD STAGE)

Disk S/N	No. of Cycles	Time (Hrs.)
6S7833(1)	6,484	*
IR2776	13,276	*
9T2898	8,539	*
P3	2,041	5,479
4S5158	13,784	*
2S4641(2)	6,458	15,558
9S0792	5,814	*
4S5078(3)	6,380	14,410
2G8945	1,112	5,562
4F5541	7,648	18,405

(1) ECP data recorded on magnetic tape for Hole F which contains two artificial slots.

(2) Holes E and G were sectioned. ECP data recorded on magnetic tape.

(3) Holes J and C were sectioned. ECP data recorded on magnetic tape.

* Unknown

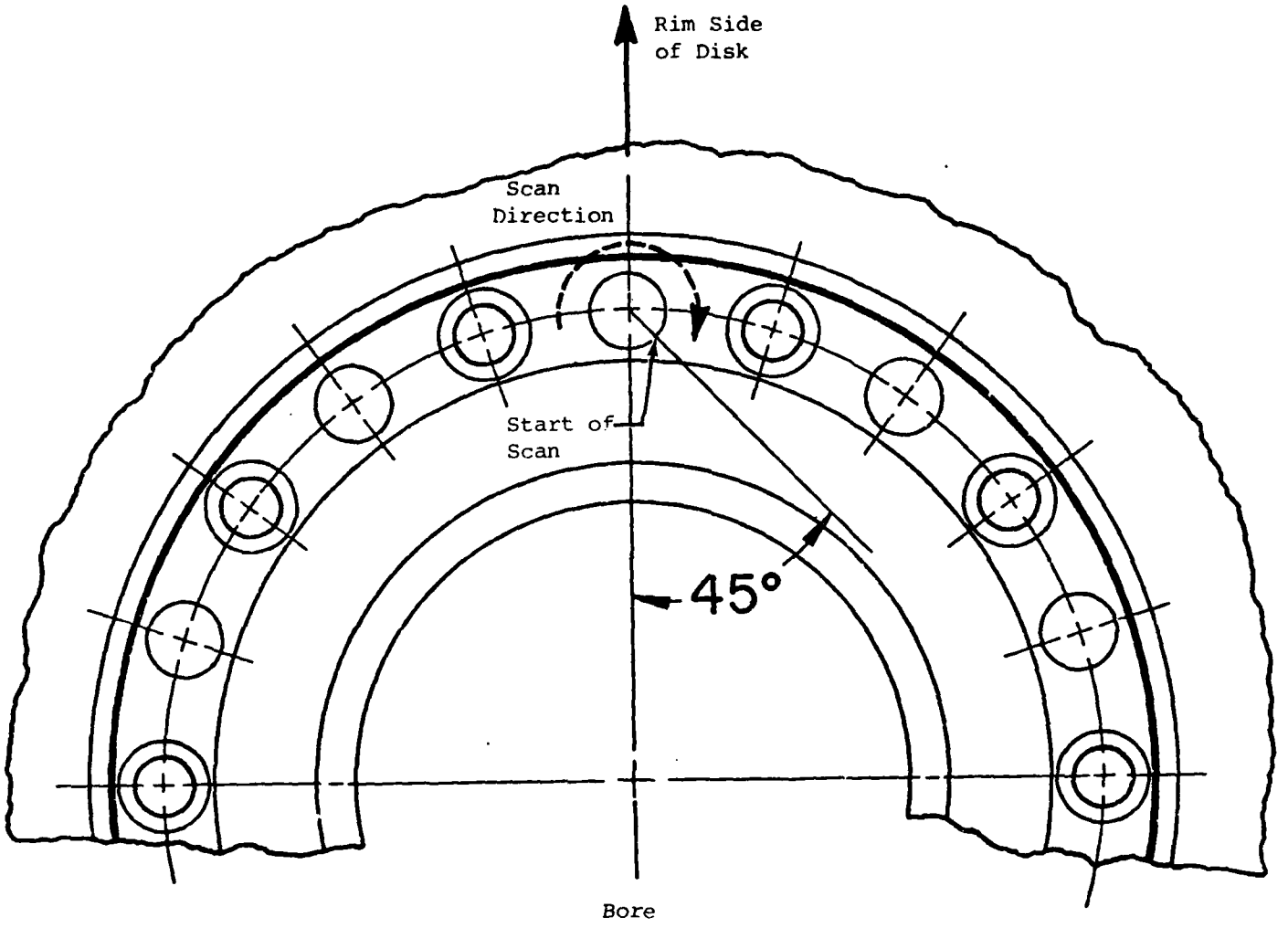

FIGURE 4. TIEBOLT HOLE SCANNING CONFIGURATION

Figure 5 as it appears on the strip-chart recording. Several sets of information are included on the chart. The signal in the bottom trace is the unfiltered ECP signature from which defect characterization can be obtained. The signature in the top trace is a filtered version of the unprocessed signature which minimizes the gradient encountered in the signal near the ends of each hole. This gradient is due to the influence of the abrupt change in disk thickness near the bore and rim side of each hole. Filtering removed most of the gradient and enhanced the signal-to-background ratio. The simple filtering circuit used here distorted the defect signatures somewhat, thus making them suitable only for crack detection and not for accurate measurement of signal characteristics. More sophisticated filtering arrangements could lessen or eliminate the distortion problem.

Since each scan covers slightly more than 6.28 rad (360^{o}), a zero reference pulse was applied to the top event marker on the strip-chart recording. This marker indicates the beginning and end of each scan as designated in the figure, and all data appearing outside of these pulses should be disregarded. On the bottom event marker channel, a 50-pulse per revolution signal is recorded to show circumferential position around the hole.

The strip-chart data recorded at 0.32 mm (12.5 mil) increments for the five selected holes are supplied as a deliverable item on this project. These data were taken at a sensitivity setting of 20 mV per small division on the unfiltered channel and 100 mV per small division on the filtered channel except for Hole J. For Hole J only, all traces are at 10 and 50 mV settings unless otherwise marked on the chart.

ECP data were recorded on analog magnetic tape (also a deliverable item) simultaneously with the strip-chart data. Data recorded includes the unfiltered ECP signal, the filtered ECP signal, the zero reference pulse, the 50 pulse per revolution markers, a data valid signal, and a voice channel identification. The data valid signal is for the purpose of automatic data processing and goes to a high level immediately before the zero reference pulse which marks the beginning of each trace and then back to a low level after the zero reference pulse which marks the end of each trace. In this manner, the entire trace is bracketed with a high level on the data valid channel. For automatic signal processing, the processing unit can be enabled only when the data valid channel is at a high level so that spurious signals associated with starting and stopping the recorder during the data taking procedure can be ignored.

Table IIA gives the channel identification for the magnetic tape data. Note that the ECP filtered and unfiltered signals and the data valid signal are recorded using a frequency modulation (FM) mode because of the low frequency nature of the signals. Magnetic tape format corresponds to the IRIG Wide Band Group 1 specifications (carrier center frequency of 6.75 KHz) and was recorded at a speed of 1 7/8 inches per second. In addition to the actual data, identification of each signal trace was put on the tape recorder voice channel. At the beginning of a new data set, the disk and hole designations are identified along with the starting position of the first scan and the ECP instrument sensitivity. For successive scans in that same hole, only the scan position measured from the top surface of the hole is recorded on the voice channel.

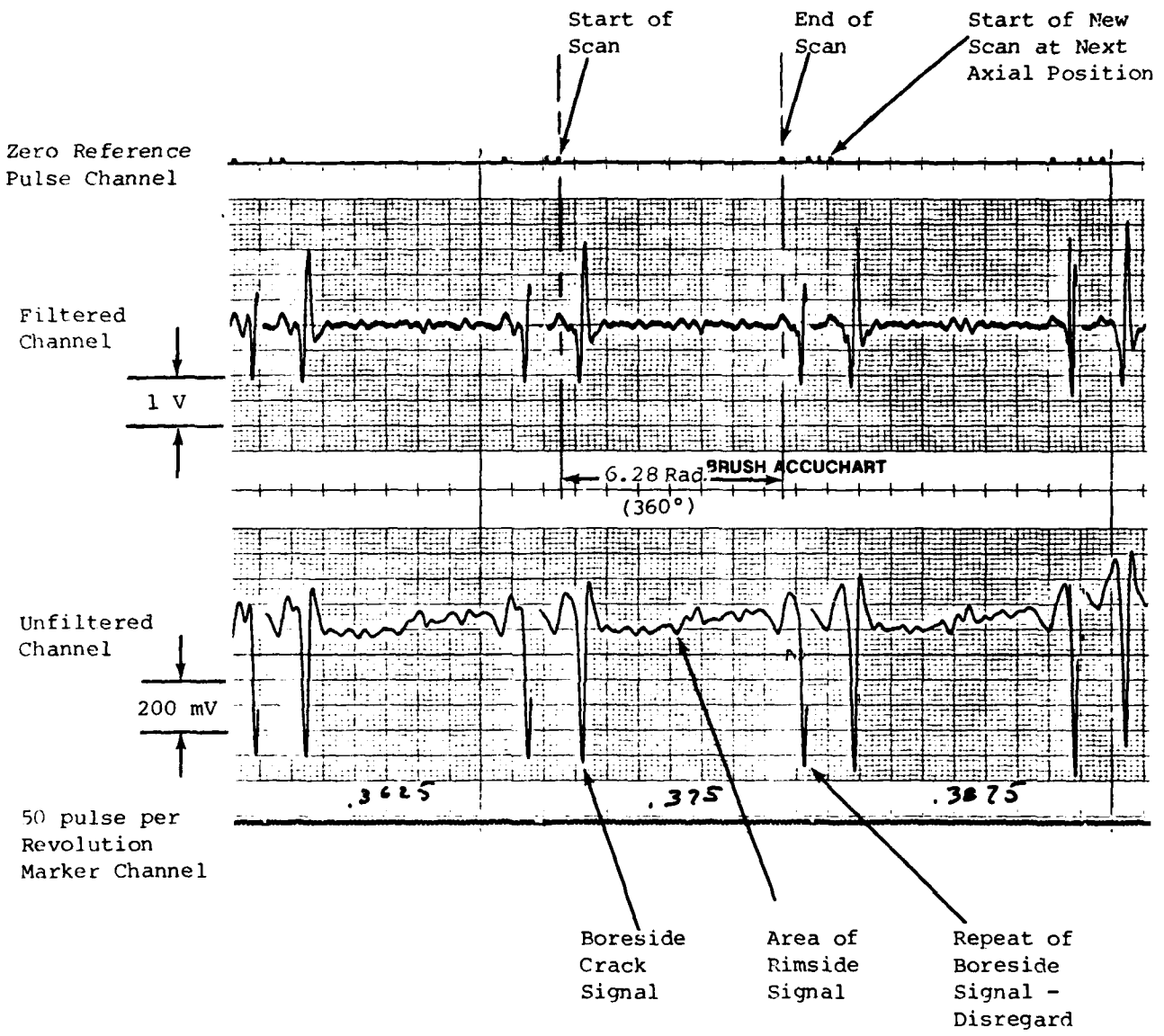

5519

FIGURE 5. TYPICAL ECP STRIP CHART RECORDINGS

TABLE II

MAGNETIC TAPE DATA

A. Channel Identification

Channel	Data	Mode
2	ECP Unfiltered Signal	FM
3	ECP Filtered Signal	FM
4	Data Valid Signal	FM
6	Zero Marker Pulse	Direct
7	Position Marker (50 pulses/rev)	Direct
Voice	Identification of Each Trace	

B. Data Sequence

Disk S/N	Hole
1. 4S5078	J
2. 4S5078	C
3. 2S4641	E
4. 2S4641	G
5. 6S7833	F

Table IIB shows the sequence on tape in which the data from each hole were recorded. The unfiltered data on magnetic tape were recorded at a gain of unity; however, the filtered signal amplitude was reduced by a factor of 10 to get it into the proper range for recording.

IV. EXPERIMENTAL RESULTS

A. ECP Signal Characteristics

ECP signals exhibit several important characteristics which are useful for defect detection and characterization. These characteristics include amplitude, polarity, and shape; excellent repeatability; and existence of repeatable signal background in non-cracked areas which is related to material characteristics. Also important is the high signal-to-electronic noise ratio.

In order to show signal characteristics which result from a defect of simple geometry, a slot was introduced normal to the bore surface of tiebolt Hole F in disk S/N 6S7833 by air-abrasive machining. This slot was then scanned at increments along its axial length to generate representative signatures. Figure 6 shows ECP signals obtained from this slot which measures 0.64 mm (25 mils) long by 0.23 mm (9 mils) deep by 0.15 mm (6 mils) wide (measurements taken from a surface replica). As the circumferential scans approach the crack along its axial length, note that a sizeable defect signature is obtained even at a distance of 1.91 mm (75 mils) from the center of the slot. At closer scans the signal builds to a maximum in amplitude and then very abruptly changes to an almost null signal over the slot center. As the scan moves past the center of the slot, the signal reverses polarity and amplitude again builds very rapidly in the opposite direction, slowly diminishing at further axial distances.

Several important defect characteristics can be obtained from these signal measurements. First, the center of the slot can be precisely located because the signal becomes null and reverses polarity at that position. In addition, the spacing between locations at which the signal is maximum is related to slot length. Signal amplitude is also very important, as previous experimental results have shown that amplitude is directly proportional to the interfacial area of the slot for small slots.

The ECP technique is highly sensitive to very small defects. Note that the ECP signatures are very large in amplitude and well defined. Although the signal background in a region away from the slot is not shown in these traces, analysis of signal background from this and various other holes in several disks shows that the signal-to-background ratio for this slot is approximately 14 to 1. Therefore, based upon the fact that signal amplitude is directly proportional to defect interfacial area it is estimated that a slot with 14% of the area of the slot in Figure 6, for example, a slot 0.25 mm (10 mils) long by 0.08 mm (3 mils) deep, could still be detected with a signal-to-background ratio of approximately 2. It was anticipated that an isolated crack could be found in one of the disks which would provide a basis for direct confirmation of the minimum size crack detectable; however, all holes examined contained several cracks which were so close together that signals could not be entirely isolated from each crack using the present probe.

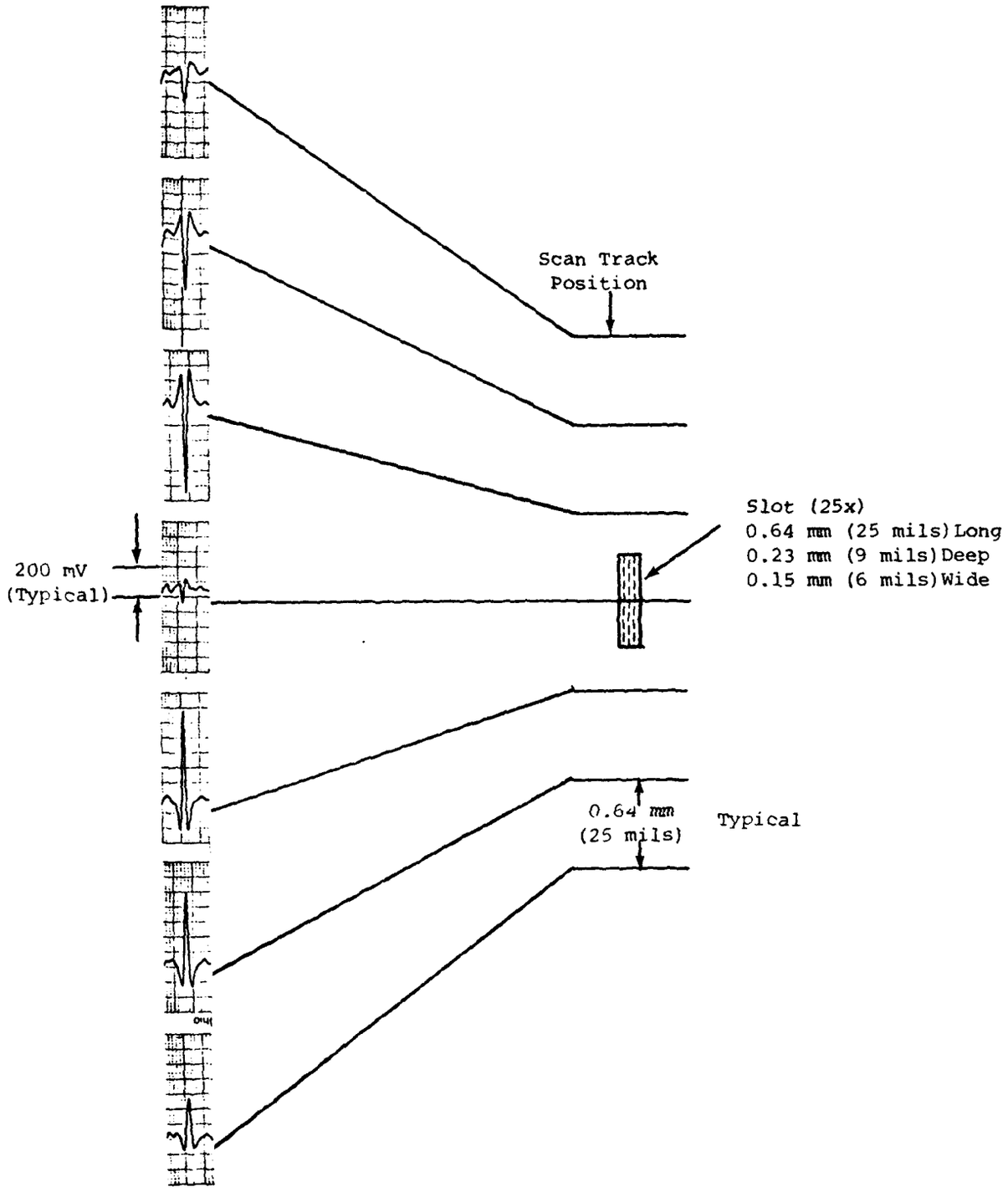

5520

FIGURE 6. ELECTRIC CURRENT PERTURBATION (ECP) SIGNATURES FROM SLOT IN TF 33 3RD STAGE TURBINE DISK TIEBOLT HOLE

Another very important feature of the ECP signals is their excellent repeatability. Figure 7A shows two repeat scans of the same scan track in the same tiebolt hole. Note that every detail of the crack signal and also of the signal background throughout the entire scan is highly repeatable, although a slight baseline drift occurred due to some instability in the rudimentary instrumentation. These data confirm that the signal and the background characteristics are precisely related to characteristics of the hole under inspection and are not due to outside influences such as might be encountered from electronic noise, probe liftoff variations, or probe wobble.

To illustrate the technique's potential sensitivity to extremely small defects, Figure 7B shows a trace made with the probe removed from the tiebolt hole and scanned in air in a normal manner with the sensitivity increased by a factor of 50 over that shown in the traces in Figure 7A. Note that even the background signals in normal scan traces are far above the electronic background noise obtained in this experiment. Thus, sensitivity is limited by material characteristics and not by system noise. This is very important since materials which are more homogeneous and have a smaller grain size (such as IN-100) should exhibit lower background signals enabling much smaller defects to be detected and characterized by the ECP method.

B. ECP Response to Closely-Spaced Slots

A significant advantage of the ECP method is the potential capability to discriminate individual cracks in regions of multiple, closely-spaced cracks. A theoretical model* which gives ECP signal characteristics as a function of defect shape and size shows that differences exist in the signatures obtained from a single and from two closely-spaced slots. These signal characteristics are most apparent in a plot of peak amplitudes of circumferential scan signatures as a function of axial position along and beyond the ends of the slots.

Theoretical predictions were calculated for a comparison between two 0.56 mm (22 mils) long by 0.20 mm (8 mils) deep slots placed end-to-end with a spacing of 0.38 mm (15 mils) and a single slot which covered the same axial length as the double slots, i.e. 1.50 mm (59 mils), and having the same aspect ratio as one of the double slots, thus yielding a large slot measuring 1.50 mm (59 mils) long x 0.55 mm (21.5 mils) deep. This represents a case where one would like to distinguish between two small slots with a relatively close spacing and a single, large defect of approximately the same combined length. Figure 8 shows the theoretical distributions of circumferential scan, peak-to-peak amplitudes versus axial position for these two situations. Note that the single large slot produces a very large difference (almost an order of magnitude) in the peak-to-peak amplitudes and also that the peak-to-peak spacing for the large slot is significantly greater than that for the two smaller slots. These important features provide a basis for identifying the two slot geometries.

*Developed under internal funding.

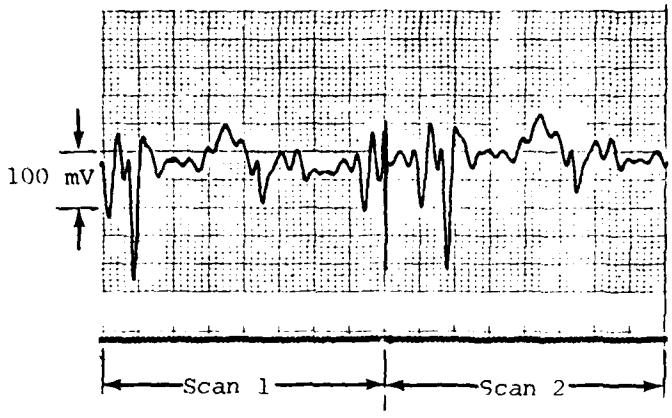

A. Repeat Scans

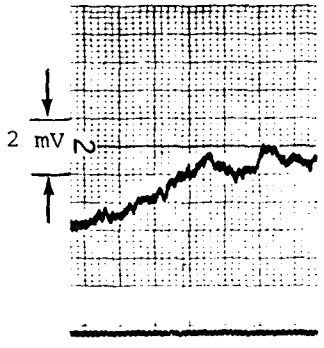

B. High Sensitivity Scan with Probe Removed From Tiebolt Hole

5521

FIGURE 7. ECP SCANS SHOWING REPEATABILITY AND ELECTRONIC NOISE

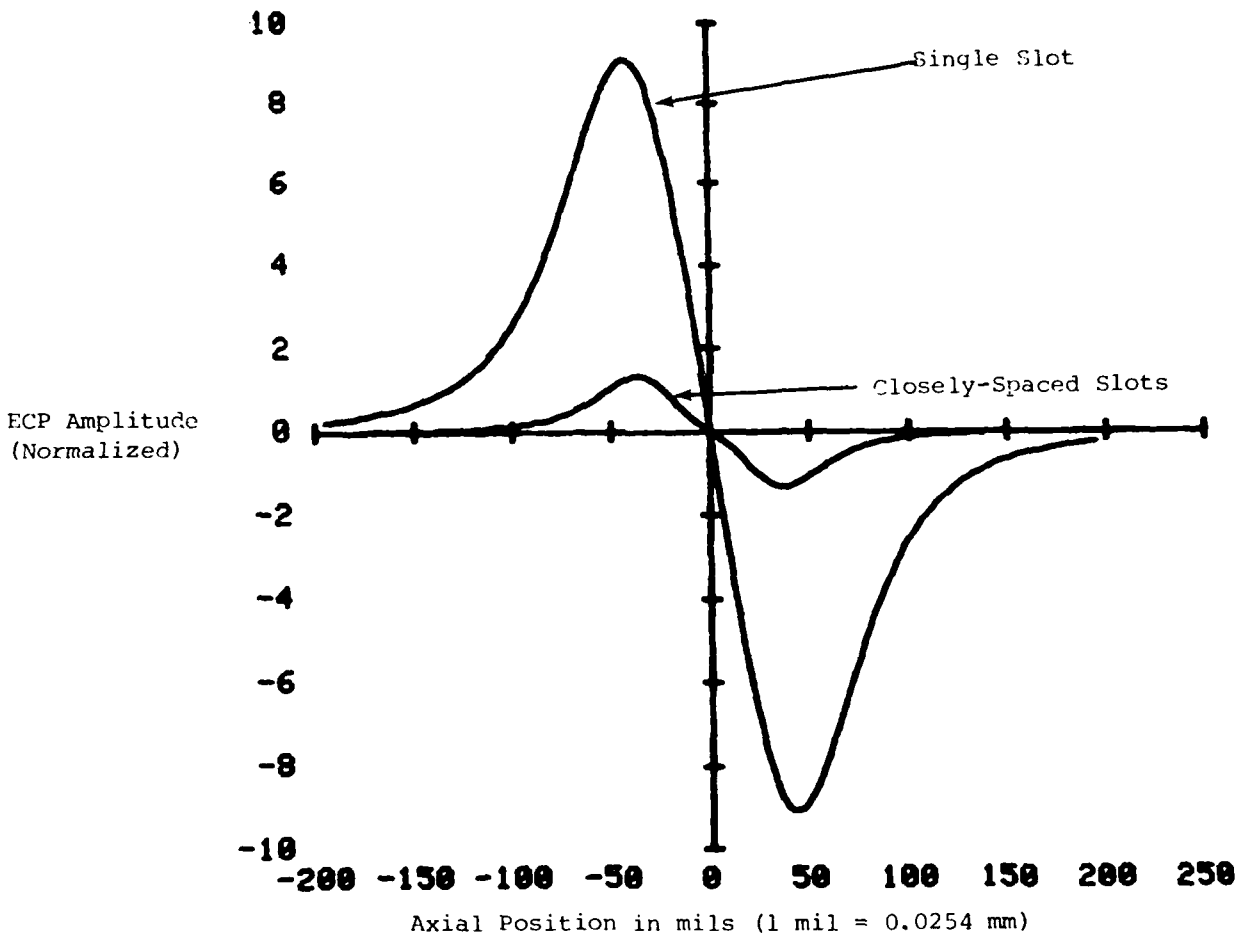

FIGURE 8. THEORETICAL ECP CIRCUMFERENTIAL SCAN PEAK SIGNAL AMPLITUDES VS. AXIAL POSITION FOR A SINGLE 1.50 mm (59 mils) x 0.55 mm (21.5 mils) SLOT AND TWO 0.56 mm (22 mils) x 0.20 mm (8 mils) SLOTS SEPARATED BY 0.38 mm (15 mils)

Another example would be the need to differentiate between two closely-spaced slots and a single slot of the same size as one of the closely-spaced slots. Figure 9 shows the theoretical prediction of the peak-to-peak amplitude distributions for this case, utilizing the same 0.56 mm (22 mils) x 0.20 mm (8 mils) slots spaced 0.38 mm (15 mils) apart and a single 0.56 mm (22 mils) x 0.20 mm (8 mils) slot. Notice again that signal features can be used to differentiate between the two conditions, i.e., the change in peak-to-peak separation and peak-to peak amplitude, and also, in the case of the two closely-spaced slots, a slight inflection of the curve in the signature region between the upward and downward peaks.

As a check on the theoretical predictions, this second case was approximated in an experiment which compared ECP signals from a single 0.64 mm (25 mils) x 0.23 mm (9 mils) slot with those from a set of two 0.61 mm (24 mils) x 0.20 mm (8 mils) slots separated by a spacing of 0.38 mm (15 mils). Figure 10 is a plot of experimental data for these two conditions with the peak amplitude of the signal from the single slot normalized to unity to obtain the same scale as in the theoretical predictions. Note that signal features in the experimental case are similar to those predicted by the theoretical model (Figure 9) with the exception of the difference in peak-to-peak amplitudes. Note also that the experimental peak-to-peak spacing is similar to that predicted by the model and that there is a slight inflection in the signal from the closely-spaced slots at the center. Some of the differences in the experimental data such as asymmetry of the positive and negative peak amplitudes can be attributed to the fact that the slots, generated by air-abrasive material removal, are somewhat irregular and are slightly different in size than was used in the modeling. Also, the slots were slightly deeper on one end than on the other as determined from replicas. These data do show, however, that the model predictions agree well with experimental data obtained from single and closely-spaced slots.

Since the slot spacing used in the previous example was very close, i.e., 60% of the slot length, another theoretical curve was generated to compare a single slot with two slots separated by a larger spacing 0.89 mm (35 mils). Figure 11 shows this comparison, and it is apparent that two slots with the larger spacing can be readily distinguished from a single slot, especially since the signal amplitudes from the two closely-spaced slots reverse polarity twice. From these evaluations it is clear that the ECP method offers significant potential for differentiating between single and multiple crack initiation.

C. Signal Correlations with Cracks

The four tiebolt holes which were selected for sectioning were examined on the surface using both an optical and a scanning electron microscope (SEM) to determine surface crack geometry. Since the cracks were very tightly closed, it was necessary to chemically etch the surface to reveal the cracks. Selected cracks and regions between cracks where indications were obtained were then sectioned metallurgically to determine subsurface crack geometry. These surface and subsurface crack geometries were subsequently compared with ECP signal features. An analysis of correlations obtained follows.

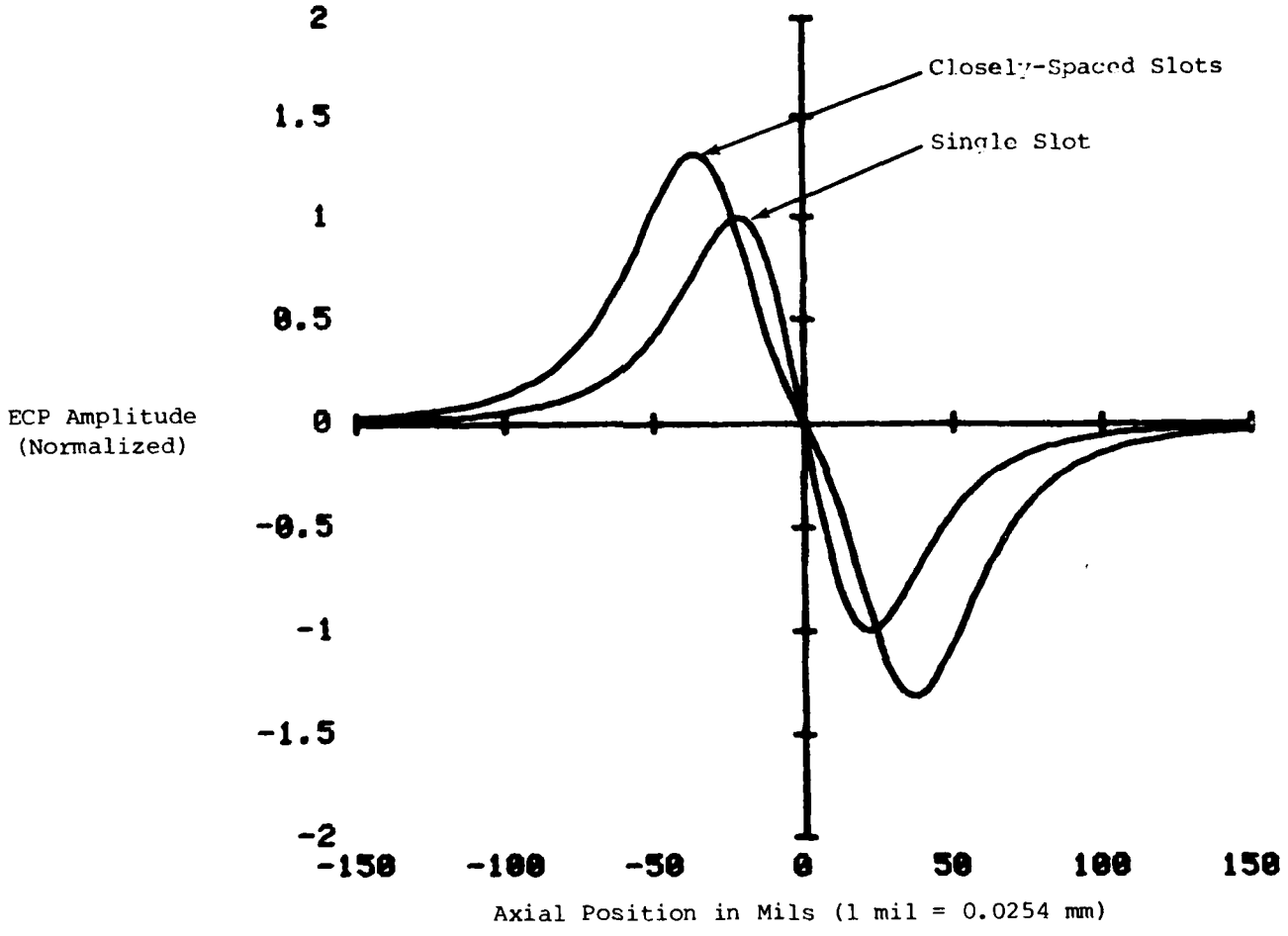

FIGURE 9. THEORETICAL ECP CIRCUMFERENTIAL SCAN PEAK SIGNAL AMPLITUDES VS. AXIAL POSITION FOR A SINGLE 0.56 mm (22 mils) x 0.20 mm (8 mils) SLOT AND TWO SLOTS OF THE SAME SIZE SEPARATED BY 0.38 mm (15 mils)

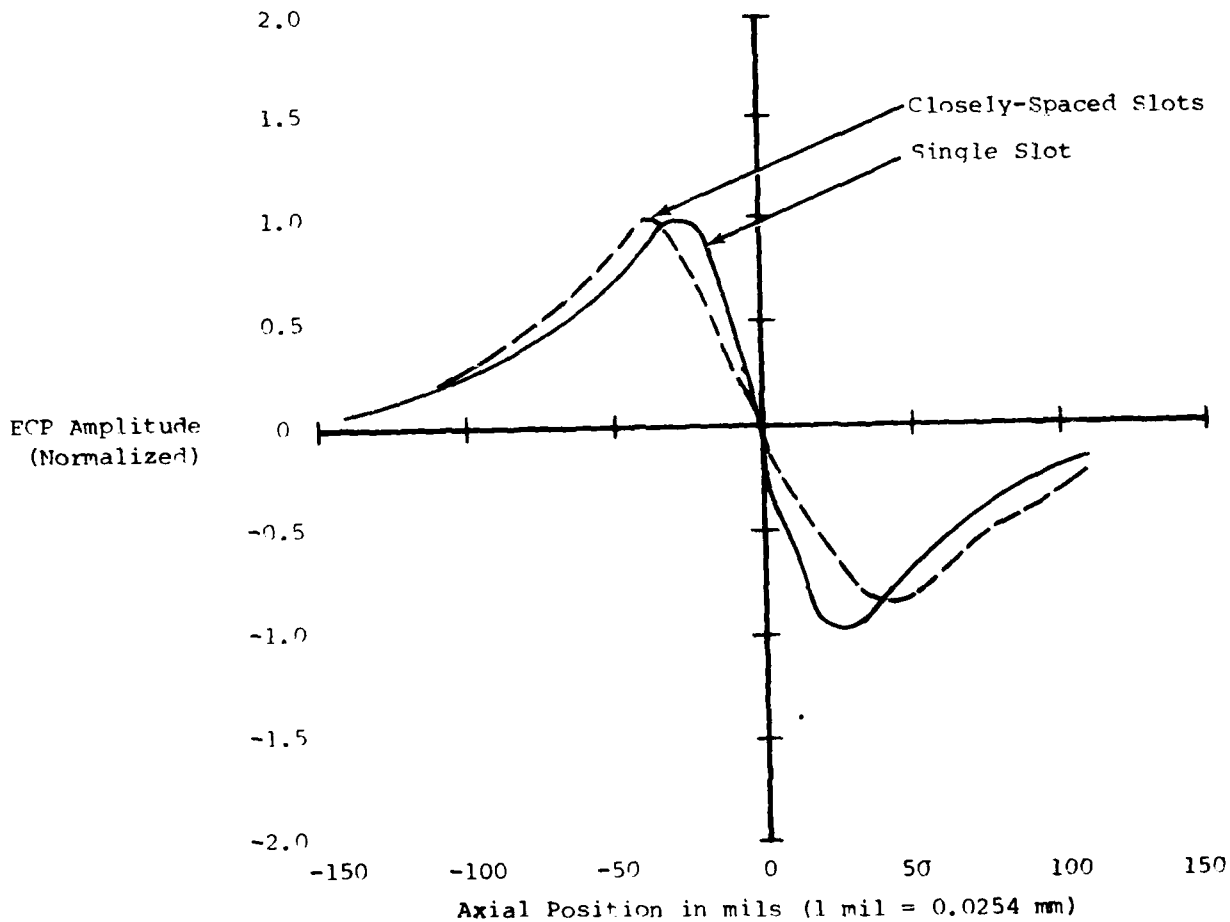

FIGURE 10. EXPERIMENTAL ECP CIRCUMFERENTIAL SCAN PEAK SIGNAL AMPLITUDES VS. AXIAL POSITION FOR A SINGLE 0.64 mm (25 mils) X 0.23 mm (9 mils) SLOT AND TWO 0.61 mm (24 mils) x 0.20 mm (8 mils) SLOTS SEPARATED BY 0.38 mm (15 mils)

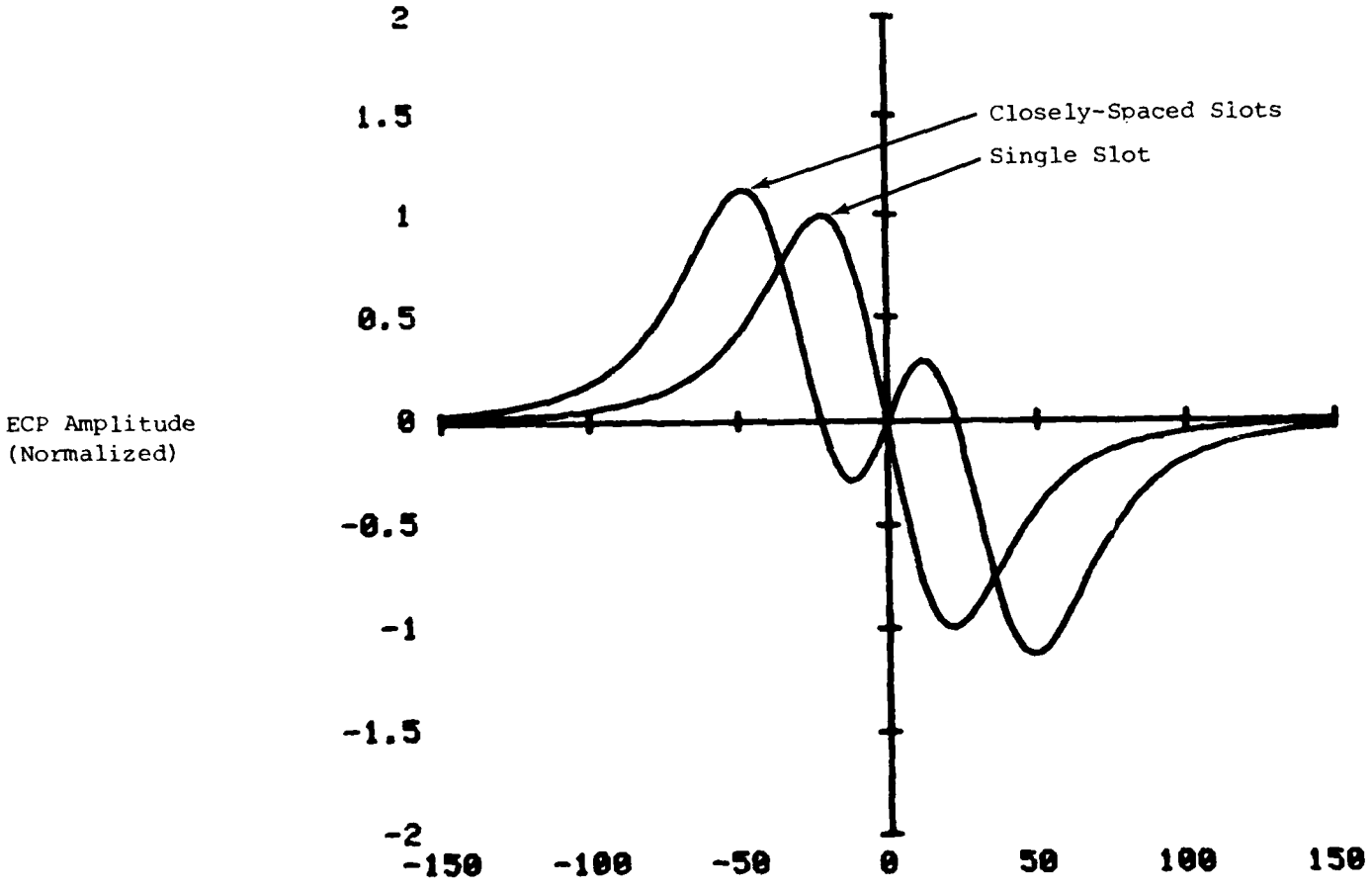

FIGURE 11. Theoretical ECP Circumferential Scan Peak Signal Amplitude vs. Axial Position for a Single 0.56 mm (22 mils) x 0.20 mm (8 mils) Slot and Two Slots of the Same Size Separated by 0.89 mm (35 mils).

Most of the sectioning results were taken from Specimen J since it showed a wide variety of crack sizes and shapes. Limited sectioning was also performed on Specimen C, and crack characteristics very similar to those in Specimen J were obtained. In each specimen, a large number of cracks spaced relatively close together were found, and in most cases the crack showed a very complex crack geometry below the surface. Many of the cracks were at an angle to the surface, some branched into multiple cracks beneath the surface, and in a few cases subsurface cracks were found with no surface indications. Many subsurface inclusions were also found.

Figure 12 shows a surface photograph of cracks near the top end of Hole J, with a sketch of the subsurface geometry of each crack; crack dimensions; and ECP signatures obtained at the designated scan track positions. Figures 13, 14, and 15 are photographs of the subsurface cross sections of each crack. Note that the ECP scans for the entire circumference of the bolt hole are shown and that the region in the photograph comprises only a small segment of the overall ECP signature. Also, since these scans are near the top of the hole, a slight gradient is still present in the signal near the center of each trace.

Because of the complex crack geometries and the close spacing of the cracks, it is believed that there exists a significant amount of signal interaction from one crack to the next with the present probe. The cracks shown in Figure 12, however, exhibit some of the simplest subsurface crack geometries of any of the cracks in the specimen. Also, Crack A is somewhat isolated (no significant cracking exists between it and the top of the hole), and it is therefore believed that the signal amplitude at its location is not greatly influenced by other cracks.

Signal analysis shows that as the ECP scans approach Crack A from the top, the ECP crack signal is first downward going (negative) and then the signal reverses polarity for successive scan track positions axially along the crack and past the bottom end. A positive polarity is then obtained near the top of Crack B. As the scan moves over Crack B and toward its bottom end, the signal again reverses polarity and also becomes broader in a circumferential direction, probably due to the influence of Crack C. The other small cracks shown in the photograph and additional cracks located further down the hole (not shown) may be influencing the signal as well.

It can be seen that the distribution of peak-to-peak amplitudes from these two cracks behaves in a manner similar to the previously presented experimental data for two closely-spaced cracks (see Figure 10). Also note that the signal amplitude obtained from Crack B is slightly larger than that obtained from Crack A due to the larger size of Crack B.

Figure 16 shows results from additional cracks at a position further into the hole, and Figures 17, 18 and 19 are the subsurface cross section photographs of each crack. Although several cracks are evident in this photograph, the response in this area appears to be dominated by Crack D, which is relatively long and deep. Note that

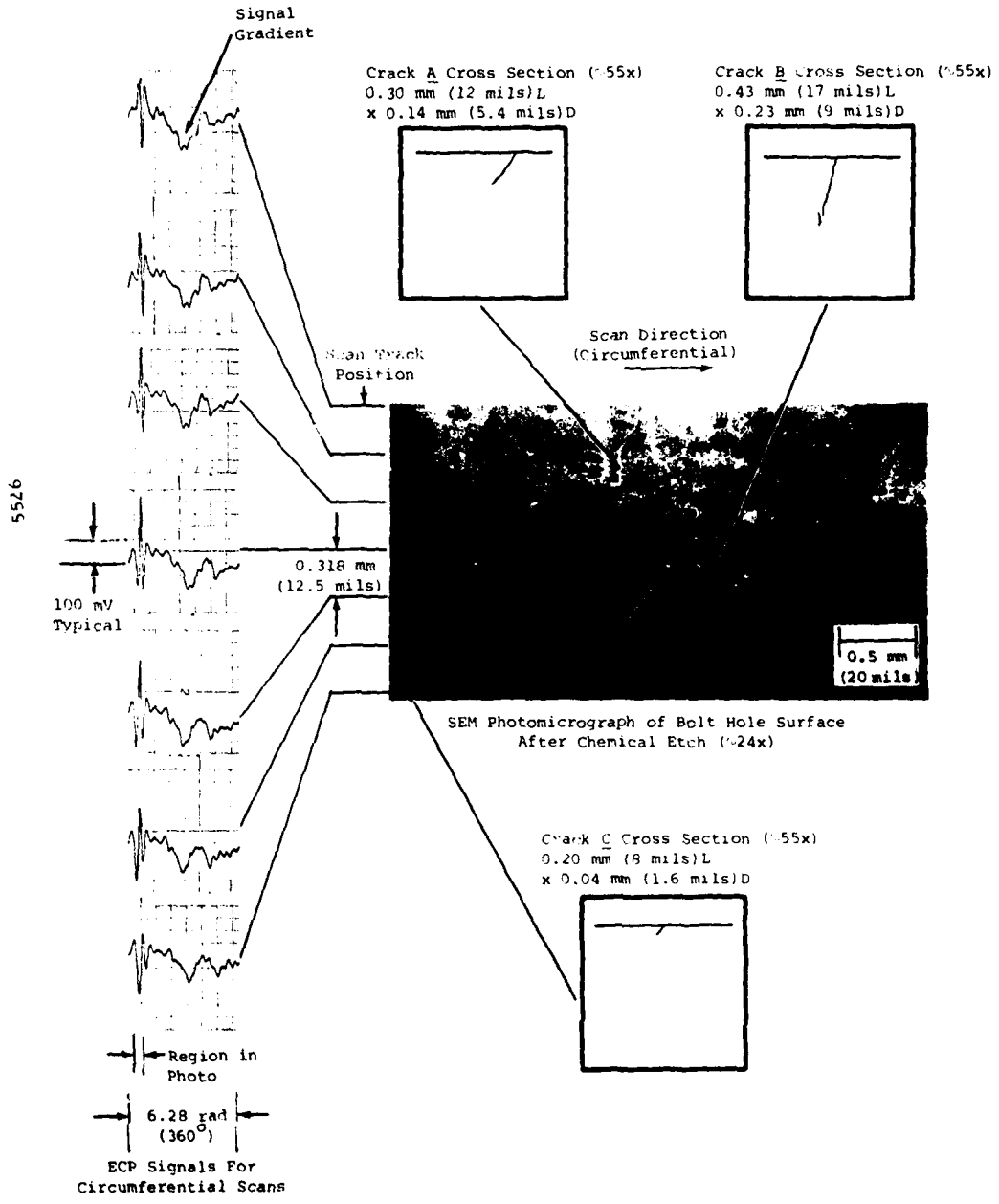

FIGURE 12. CORRELATION OF SURFACE PHOTOMICROGRAPH, CROSS SECTIONAL SKETCHES AND ECP SIGNALS FOR CRACKS A, B, AND C IN SPECIMEN J

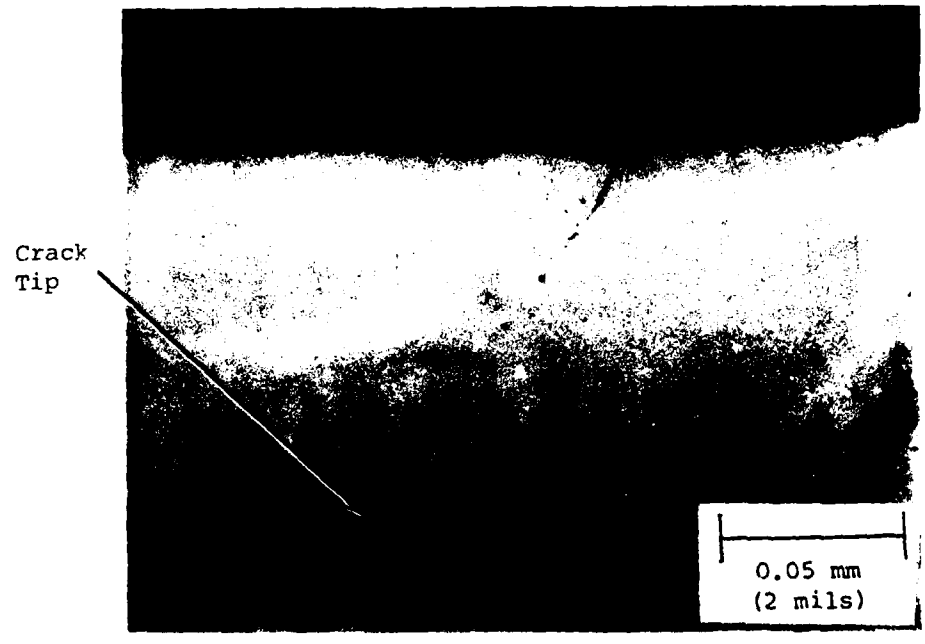

5527

FIGURE 13. OPTICAL PHOTOMICROGRAPH OF CRACK A CROSS SECTION (∿500x)

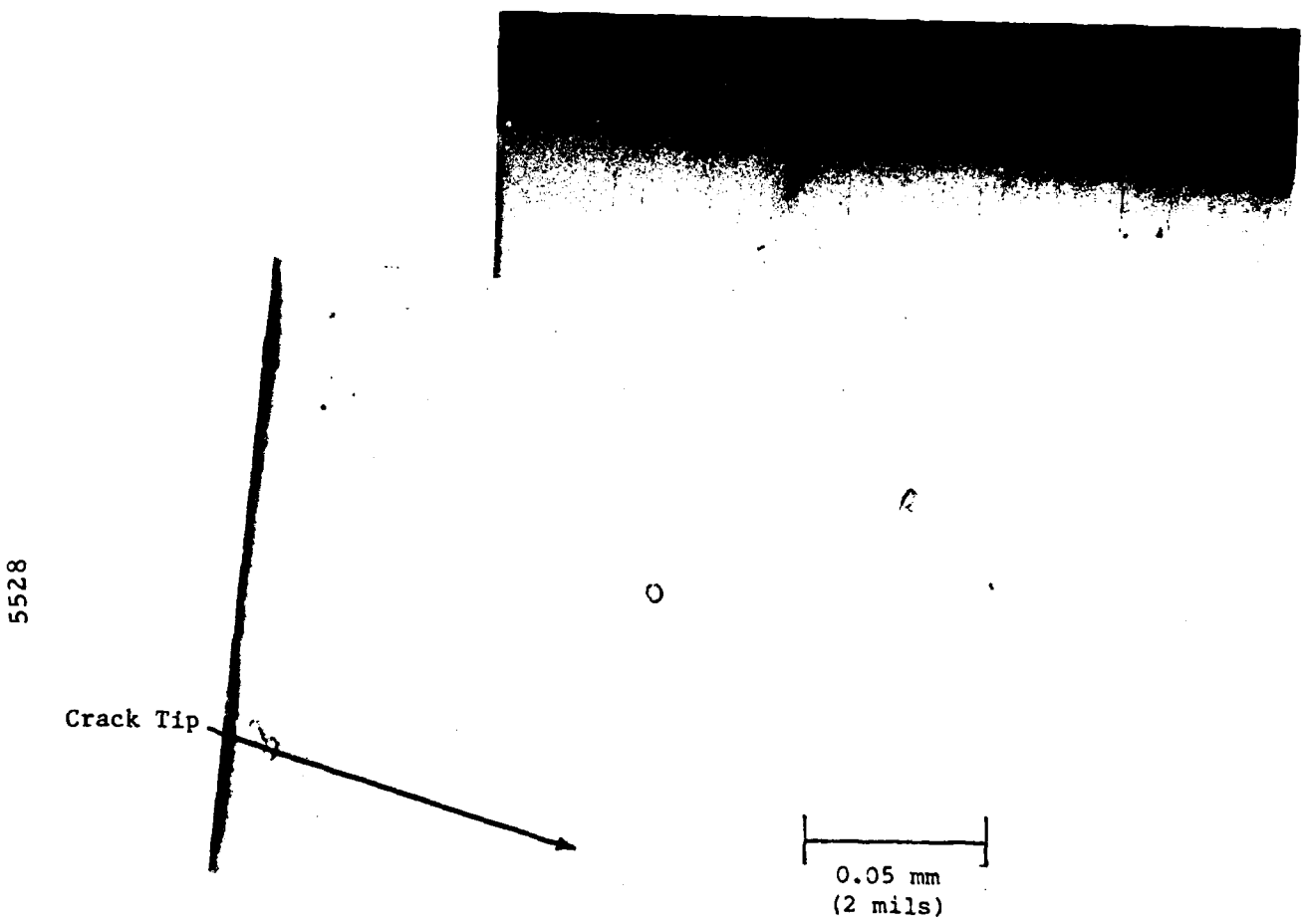

FIGURE 14. OPTICAL PHOTOMICROGRAPH OF CRACK B CROSS SECTION (∿500x)

FIGURE 15. OPTICAL PHOTOMICROGRAPH OF CRACK C CROSS SECTION (∿500x)

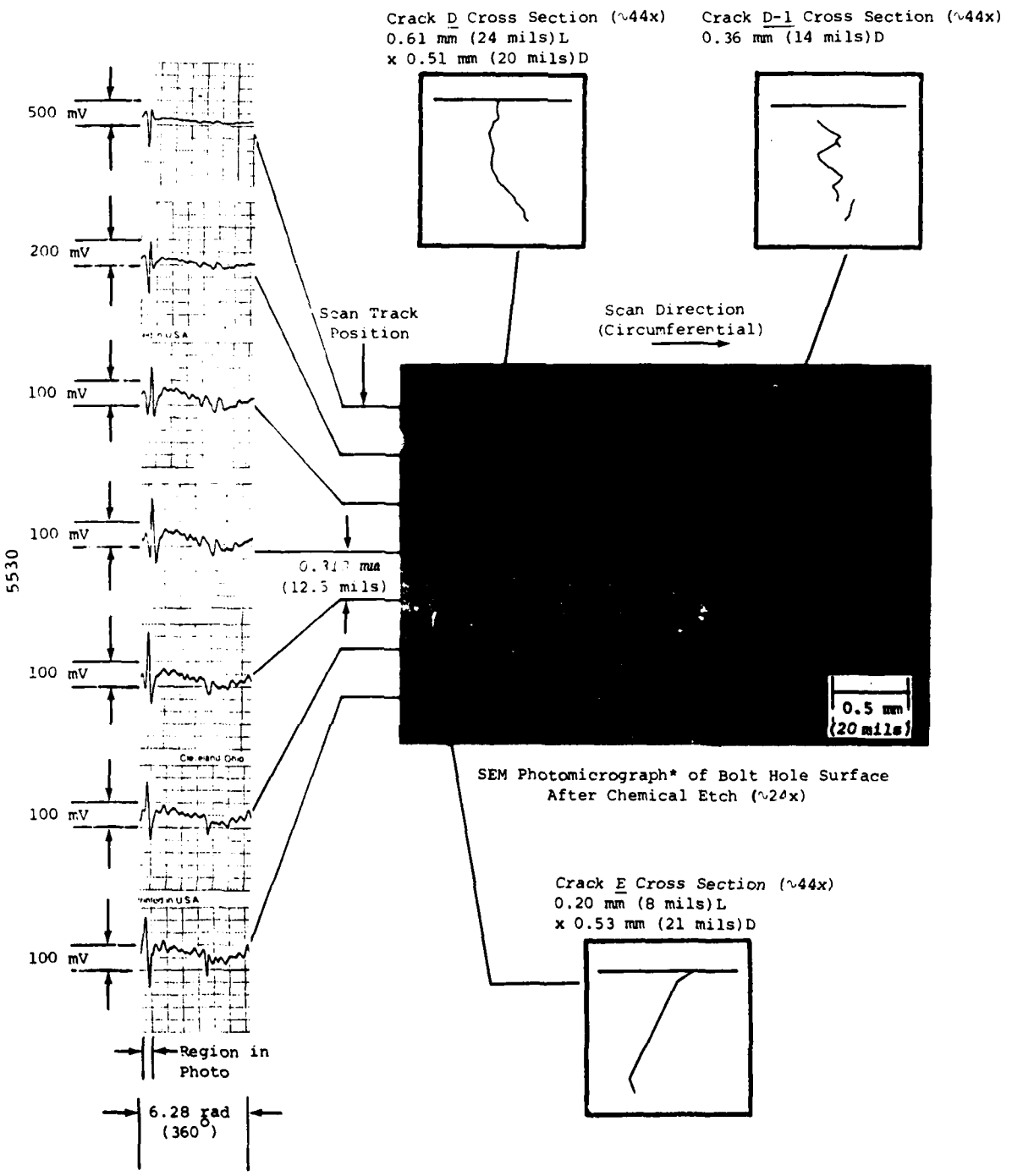

FIGURE 16. CORRELATION OF SURFACE PHOTOMICROGRAPH CROSS SECITONAL SKETCHES AND ECP SIGNALS FOR CRACKS D, D-1, AND E IN SPECIMEN J

* The difference in photomicrograph shading is due to contrast changes between multiple SEM photomicrographs.

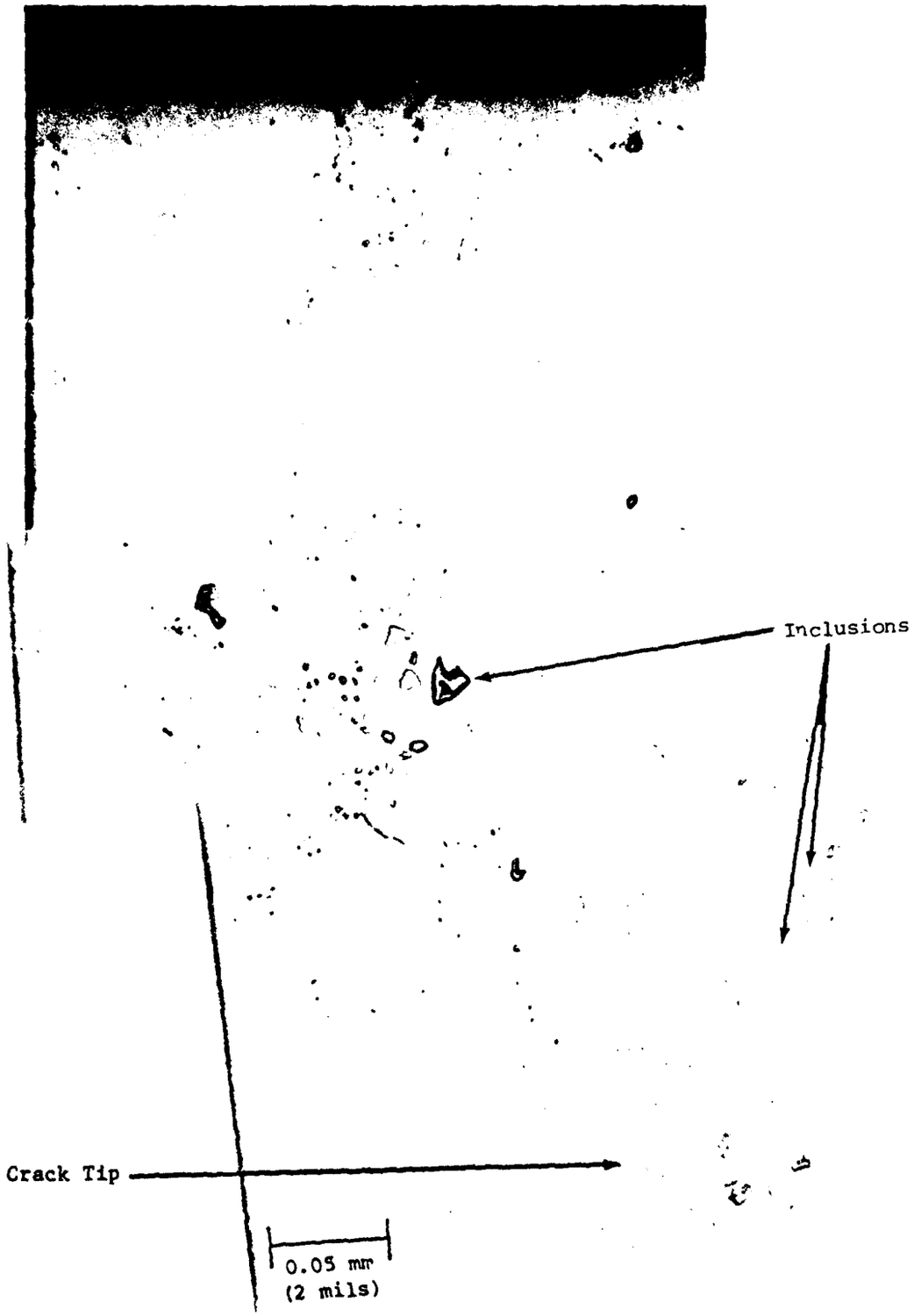

5531

FIGURE 17. OPTICAL PHOTOMICROGRAPH OF CRACK D CROSS SECTION (∿400x)

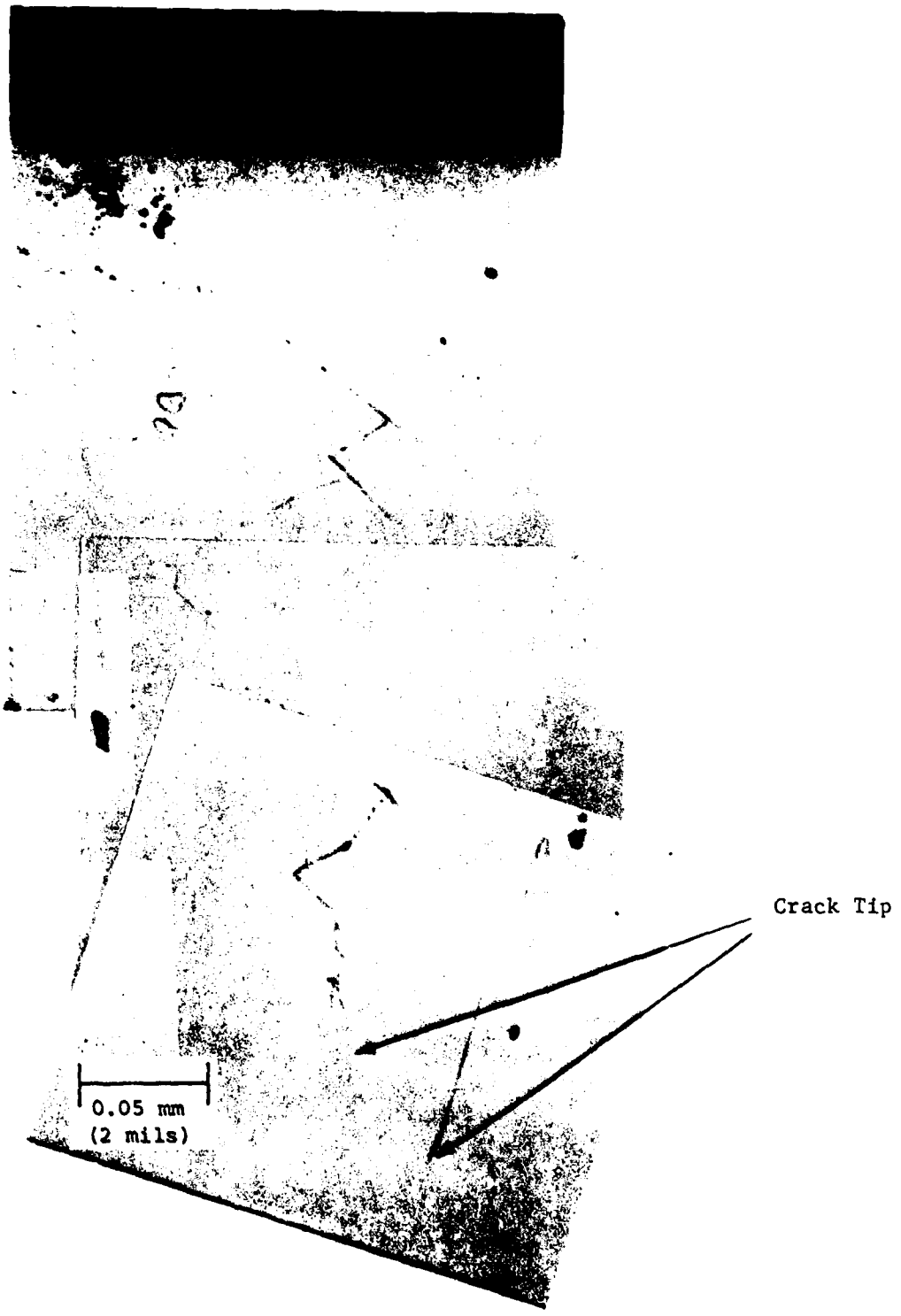

5532

FIGURE 18. OPTICAL PHOTOMICROGRAPH OF CRACK D-1 CROSS SECTION (∿400x)

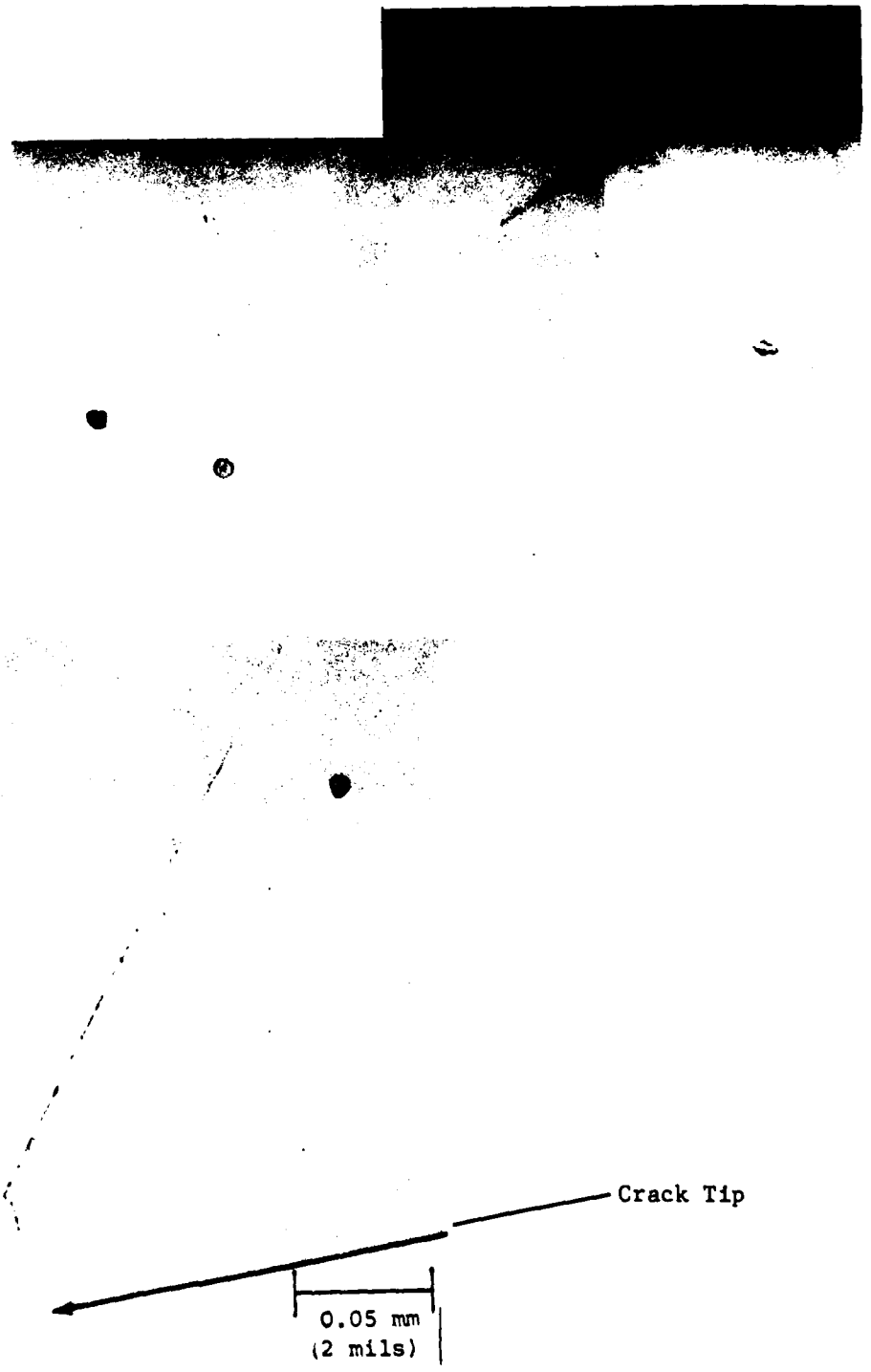

5533

FIGURE 19. OPTICAL PHOTOMICROGRAPH OF CRACK E CROSS SECTION (∿400x)

signal polarity reversal is obtained in the region of this crack. Other interesting crack characteristics are also shown in this figure. For example, Crack D-1 has no surface indication at all and could possibly be a continuation of Crack D under the surface. Also note the complicated subsurface geometry of Crack D-1. Crack E, which has a very short surface length, exhibits unusually great depth. It can also be seen that near the bottom of the photograph (Figure 16) the signal is bipolar. The concentration of deep cracks in this region and the fact that subsurface cracking exists with no apparent surface indication undoubtedly contributes to the complex signal characteristics in this region. Cracks which exist past the ends of the photograph may further contribute to signal complexity.

Figure 20 shows another region of Hole J where several more cracks exist in proximity, and Figures 21, 22 and 23 are the crack cross section photographs. Near the top of the photograph in Figure 20 the signal is bi-polar in characteristic, indicating interaction between two crack signatures. The negative portion of the bi-polar signal could be a component of the signature from Crack F, which reverses polarity and becomes positive as the scan position moves to the bottom end of the crack. Some broadening of the circumferential width of the crack signature is introduced by Crack H, which is at a different circumferential position than Crack F. Although no distinct signal indication was obtained which distinguishes between Cracks F and G, the spacing between these cracks is very close as compared to their lengths, and also Crack G is much deeper than it is long, indicating that the entire crack length may not be evident on the surface. The subsurface view of Crack H is also interesting in that a short crack indication was obtained immediately below the surface and several long indications were obtained at a significantly greater depth below the surface.

Data for the next set of cracks in Specimen J are shown in Figure 24 with crack cross section photographs shown in Figures 25, 26, and 27. Although two surface crack indications were obtained in this region, there appears to be a high degree of subsurface cracking throughout the entire area. Note that Crack I has one surface-connected portion and another very large, completely subsurface region. Crack I-1 has no surface indication at all, but exhibits three areas of subsurface cracking. Crack J has only a small surface indication, but a relatively large subsurface depth. It is possible that the deep subsurface cracking shown in all three of these cross sections could, in fact, be one portion of a large network of subsurface connected cracks. Unusual ECP signal characteristics were also obtained in this region, probably due to the high degree of subsurface cracking. Note that the signal is always positive going at all increments along the crack and does not reverse polarity; however, the signal does build to a maximum in the region of Crack I, which has the longest subsurface indication that is still connected to the surface.

A number of crack sections were also performed on Specimen C, which showed a clustering of cracks in several regions along the hole. The crack geometries in Specimen C were similar to those in Specimen J in that a large number of surface indications were present and the subsurface crack geometries were very complex. Also, subsurface cracking not evident on the surface was present on Specimen C. Since these results were very similar to Specimen J, data are not shown.

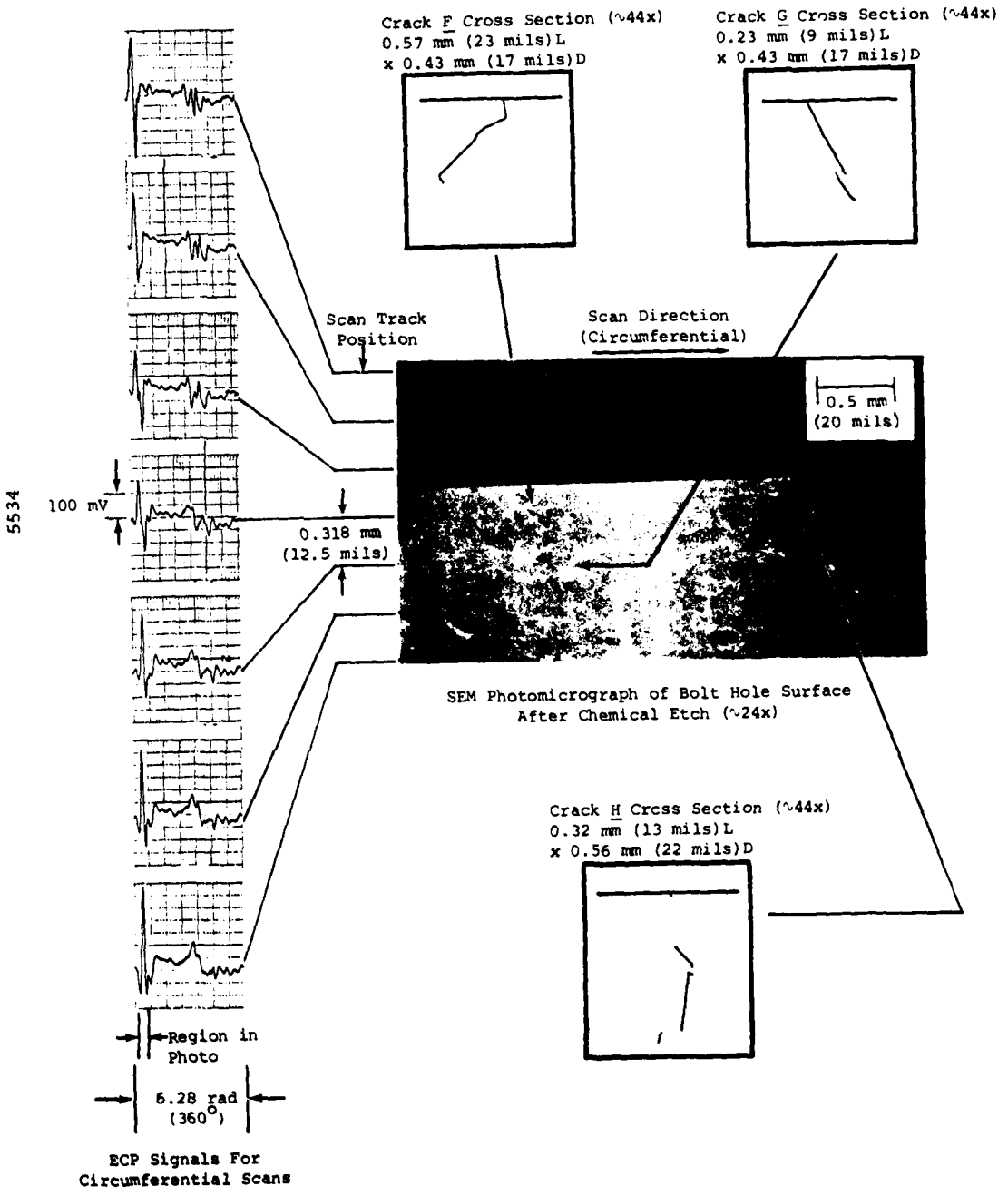

FIGURE 20. CORRELATION OF SURFACE PHOTOMICROGRAPH, CROSS SECTIONAL SKETCHES AND ECP SIGNALS FOR CRACKS F, G, AND H IN SPECIMEN J

* The difference in photomicrograph shading is due to contrast changes between multiple SEM photomicrographs.

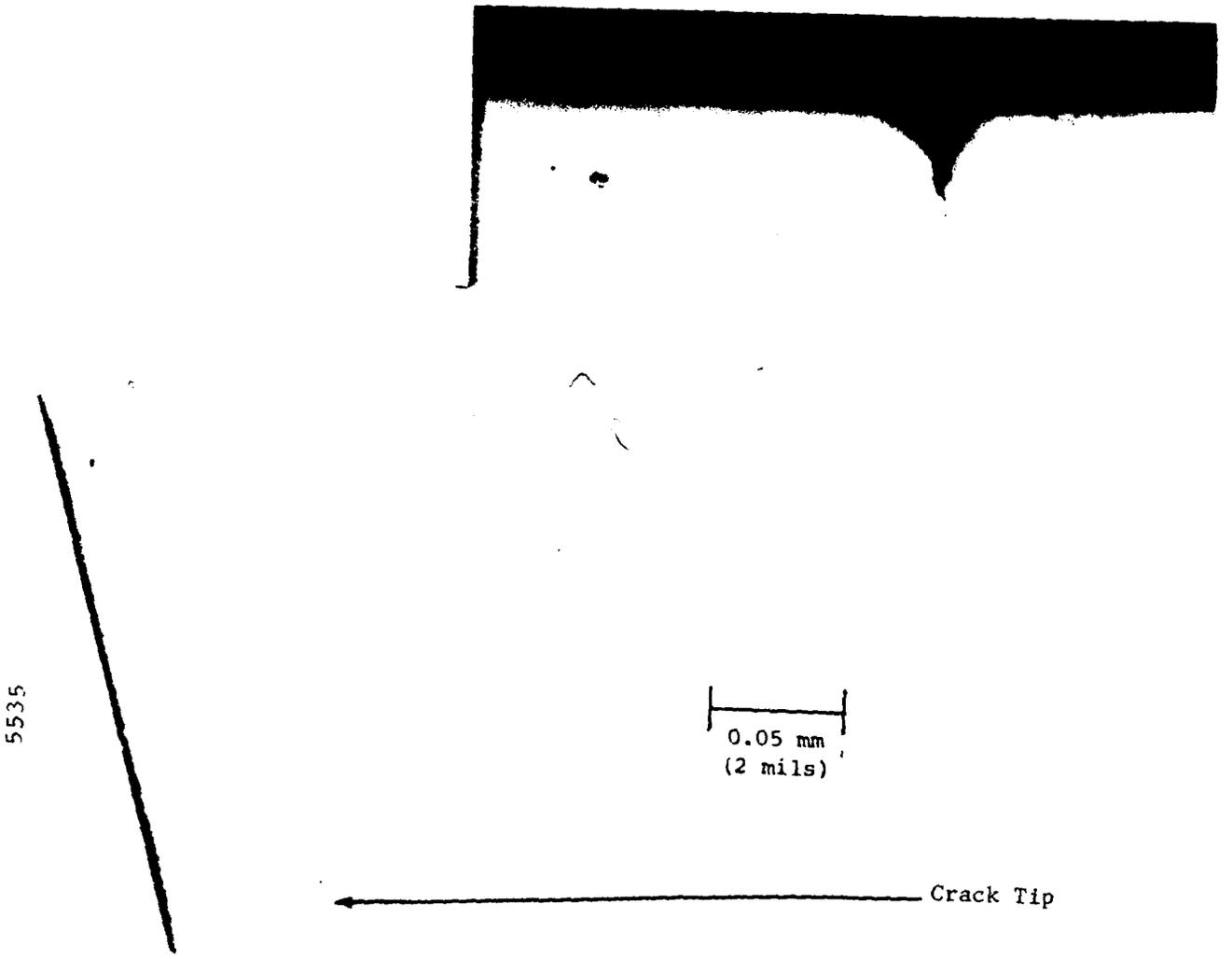

FIGURE 21. OPTICAL PHOTOMICROGRAPH OF CRACK F CROSS SECTION (~400x)

5536

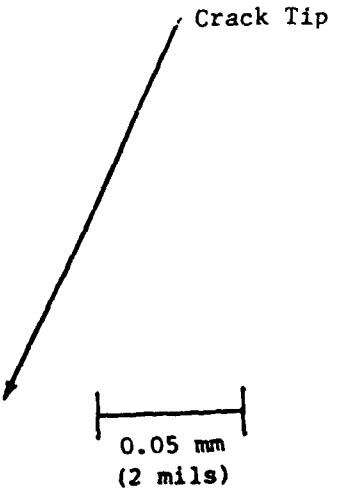

FIGURE 22. OPTICAL PHOTOMICROGRAPH OF CRACK G CROSS SECTION (∿400x)

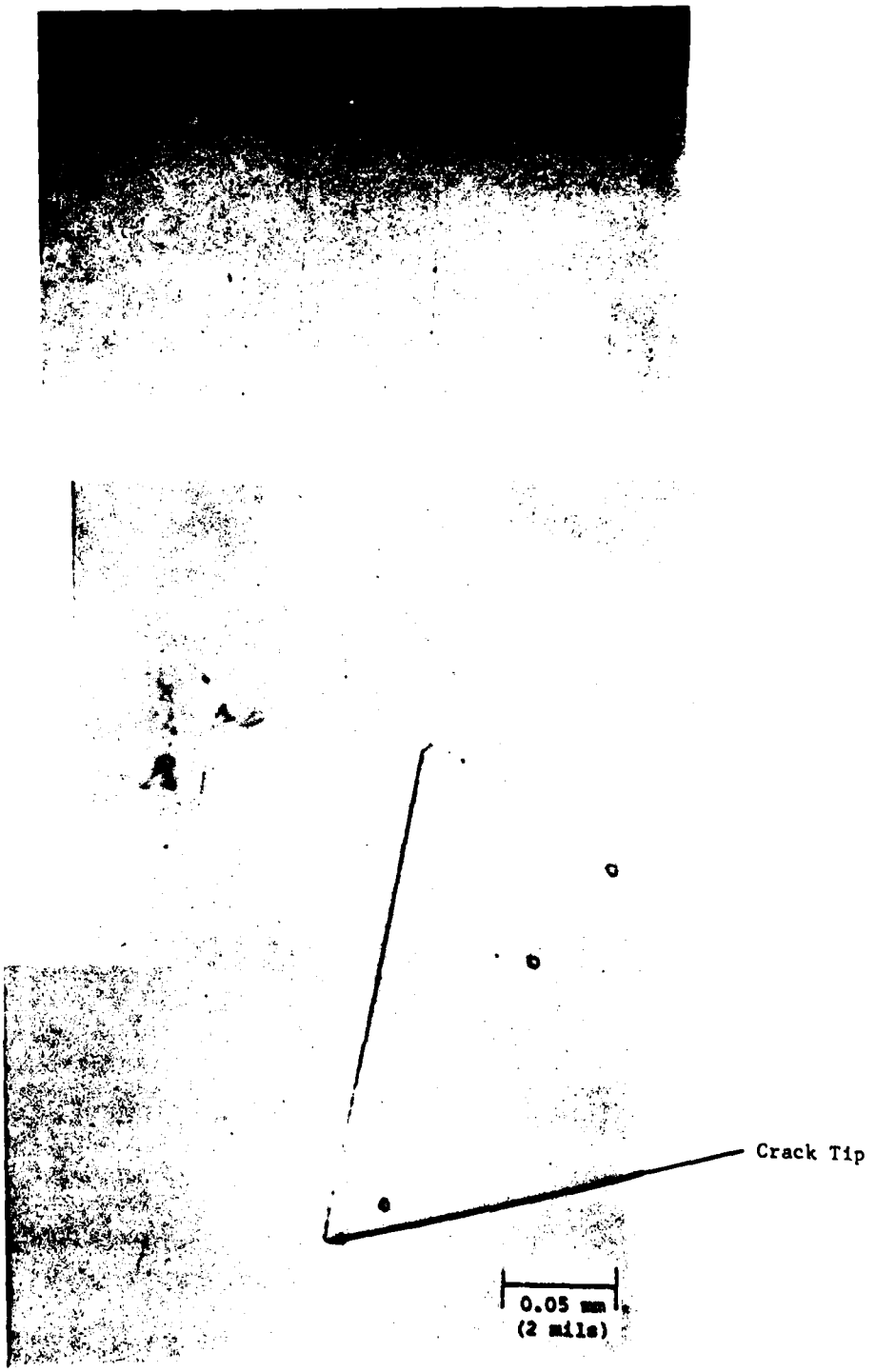

FIGURE 23. OPTICAL PHOTOMICROGRAPH OF CRACK H CROSS SECTION (∿400x)

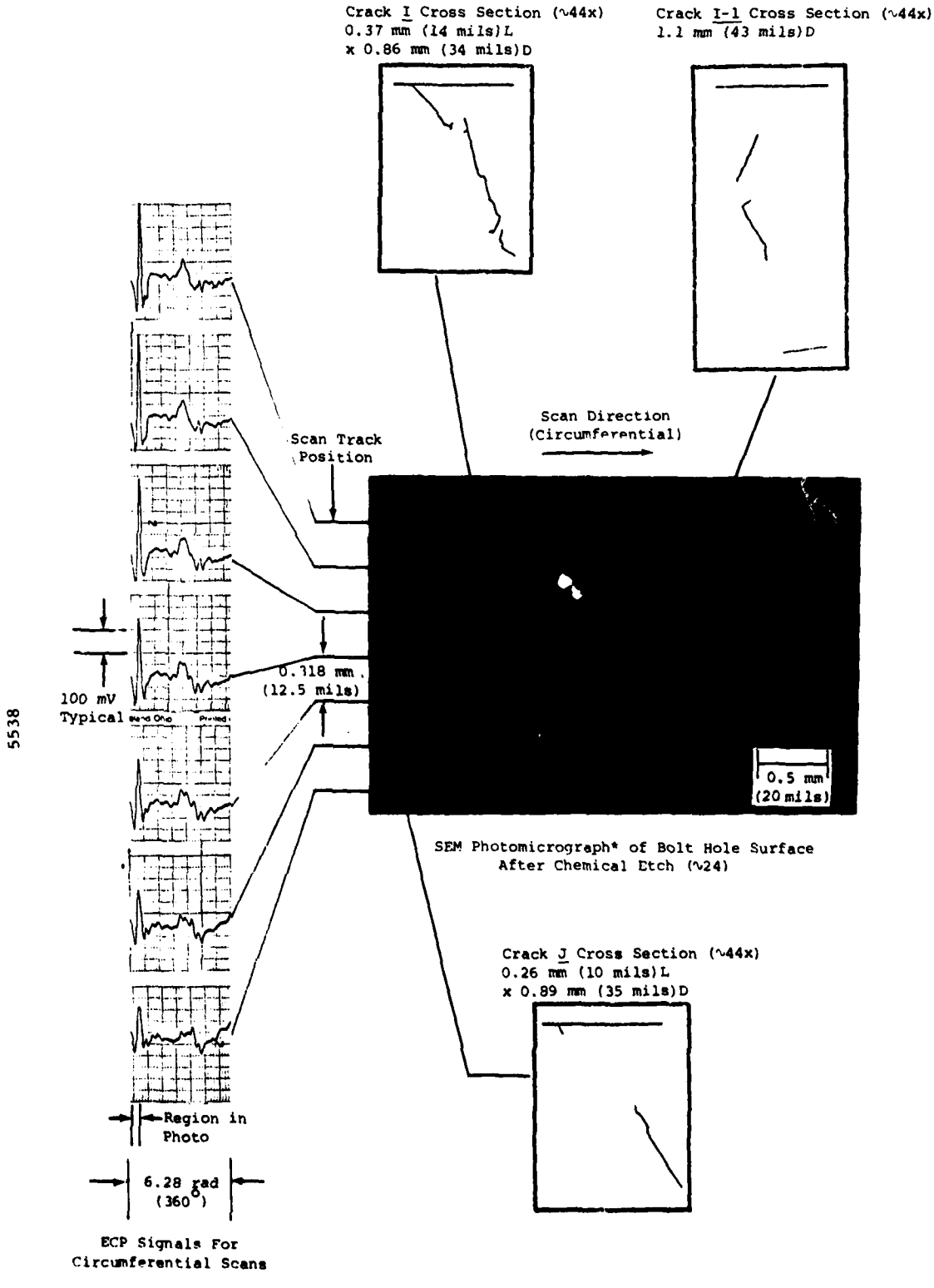

FIGURE 24. CORRELATION OF SURFACE PHOTOMICROGRAPH, CROSS SECTIONAL SKETCHES AND ECP SIGNALS FOR CRACKS I, I-1, AND J IN SPECIMEN J

* The difference in photomicrograph shading is due to contrast changes between multiple SEM photomicrographs

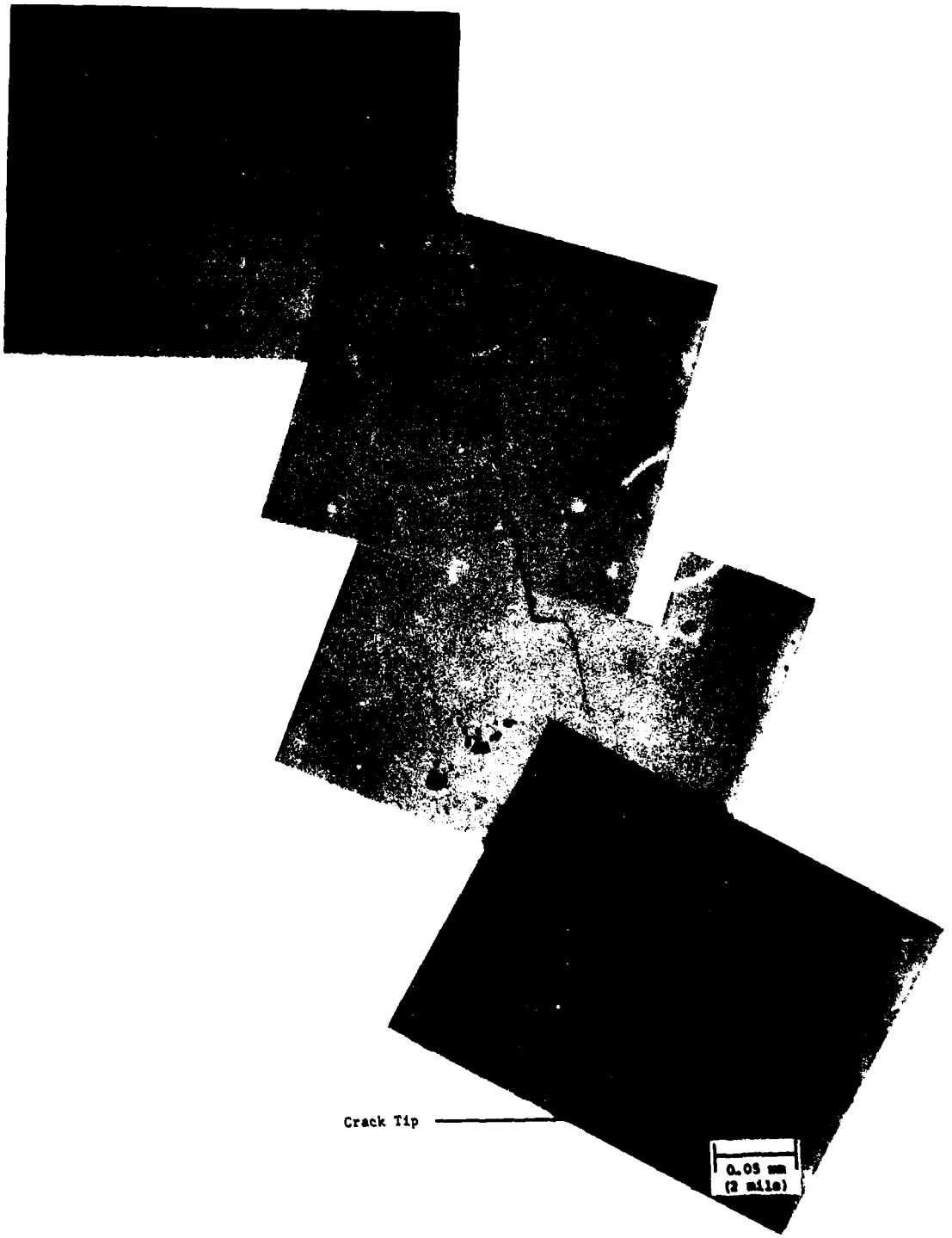

FIGURE 25. OPTICAL PHOTOMICROGRAPH OF CRACK I CROSS SECTION (~256x)

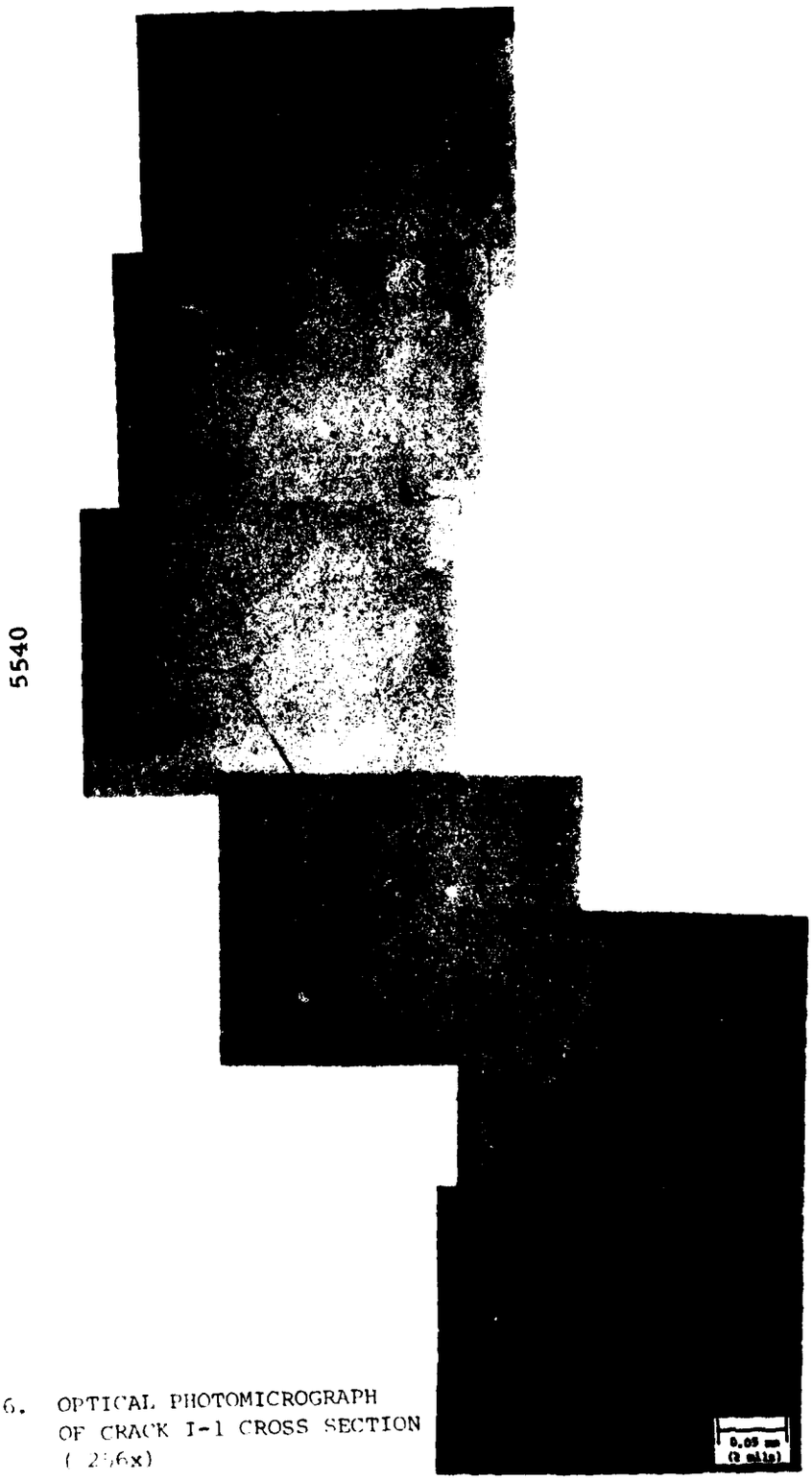

FIGURE 26. OPTICAL PHOTOMICROGRAPH OF CRACK I-1 CROSS SECTION (256x)

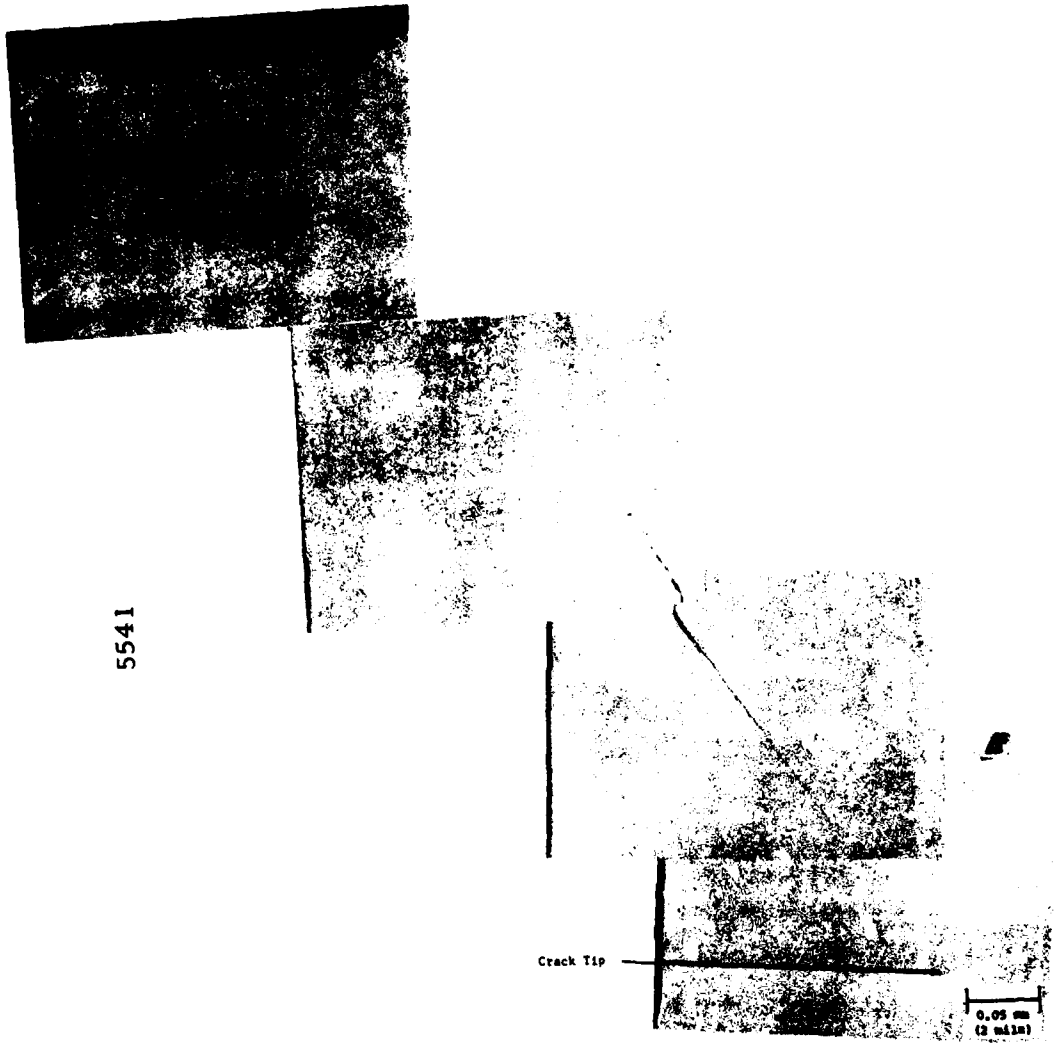

FIGURE 27. OPTICAL PHOTOMICROGRAPH OF CRACK J CROSS SECTION (∿256x)

D. Data Imaging

As an example of potentially more useful and easier to interpret data presentations than strip-chart recordings, two data imaging approaches were evaluated (under internal funding) and preliminary results follow.

The first approach consisted of an A-scan image where a series of ECP signatures were displayed simultaneously on a cathode ray tube. Figure 28 shows two views of this data presentation on Hole F which contains both the 0.64 mm (25 mils) x 0.23 mm (9 mils) slot and also a fatigue crack as designated in the figure. Figure 28A shows a series of closely-spaced scans in a region around the center of the defects while Figure 28B shows the same scans at a coarser spacing used to separate signal features. This type of presentation can be very useful since signal features on a series of scans can be viewed simultaneously, and important characteristics such as signal reversals and signal amplitude changes can be seen as a distribution along the axial length of the defect.

Another potentially useful imaging technique is a C-scan display in which the signal amplitudes are represented by shades of gray scale. The photograph in Figure 29A shows the C-scan presentation of the entire length of the hole and approximately one-half its circumference. The white areas in the photograph represent regions of maximum negative signal polarity while the black regions represent regions of maximum positive polarity, and shades of gray represent intermediate regions. The crack signature is on the left and the slot signature is on the right. Notice that the crack signature is relatively complex, while the slot signature shows distinctly the signal reversal in the rapid change from white to black. The image is somewhat smeared horizontally due to difficulties in precisely synchronizing the display with the ECP data with the rudimentary setup used here. Also, the horizontal dark bands in the photograph were caused by D.C. offsets in the data signals and are of no significance in the data interpretation. These problems can be easily corrected with additional system refinement. The photograph in Figure 29B shows an expanded view of the slot signature region where the distinct polarity reversal can be seen.

These data imaging techniques and possibly others, including correlation processes used to relate signal characteristics from unknown cracks to those of known cracks and thus determine parameters of crack geometry, could be very useful in rapidly interpreting ECP data.

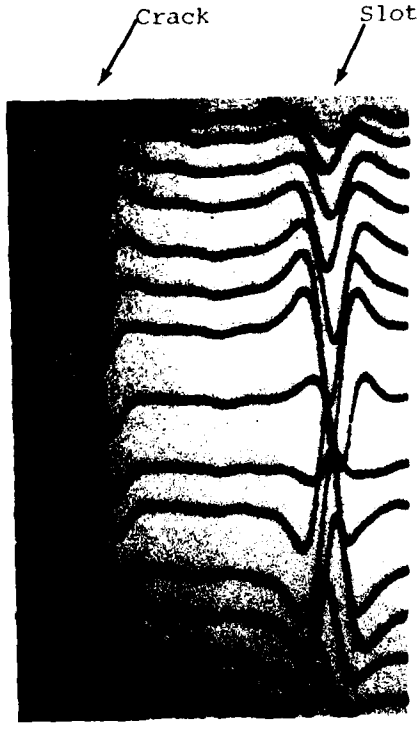

A. Compressed View

5542

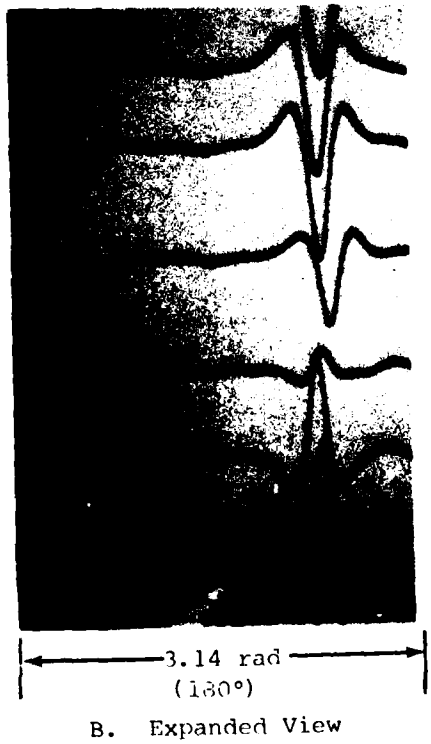

B. Expanded View

FIGURE 28. A-SCAN IMAGES OF ECP SIGNATURES FROM HOLE F, DISK 6S7833 SHOWING A CRACK AND A SLOT. SCAN SPACING IS 0.32 mm (12.5 mils)

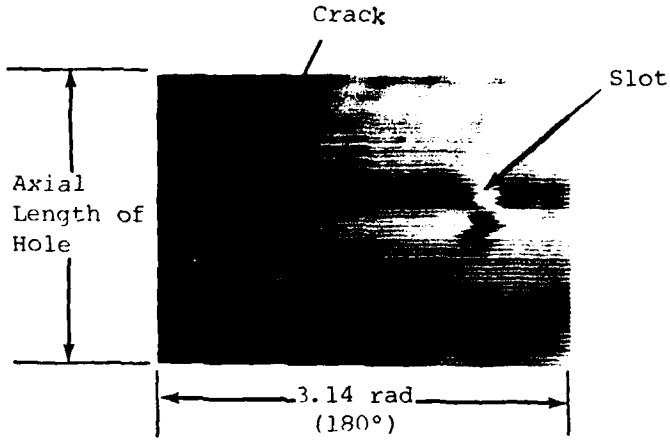

A. ECP Image from Crack and Slot

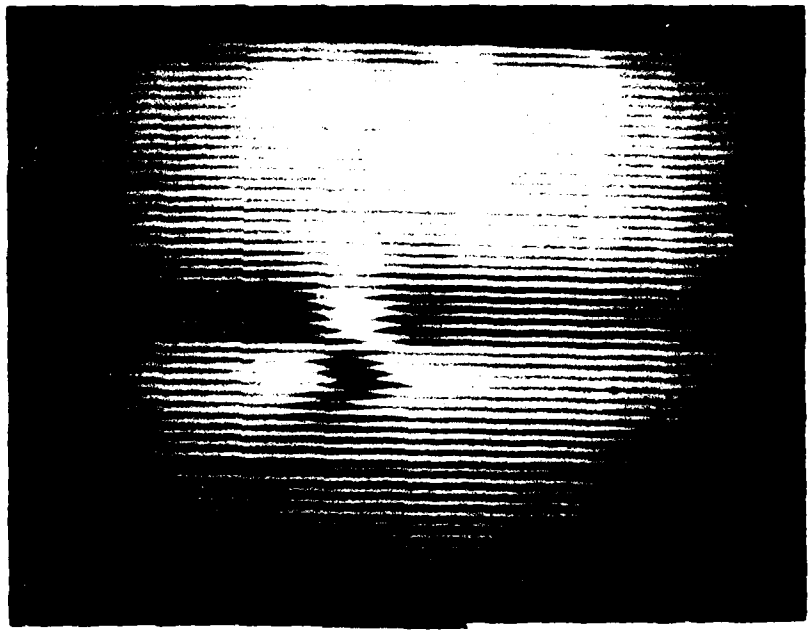

B. Expanded View of Slot Image (Above)

5543

FIGURE 29. C-SCAN PRESENTATIONS OF ECP SIGNATURES FROM HOLE F, DISK 6S7833 SHOWING A CRACK AND A SLOT

V. CONCLUSIONS

From analyses of the data obtained during this investigation, the following conclusions are drawn:

(1) The ECP method is capable of detecting very small fatigue cracks. A relatively isolated crack measuring 0.30 mm (12 mils) long by 0.15 mm (5.4 mils) deep was detected in a TF-33 turbine disk tiebolt hole. Smaller cracks were also detected; however, their signals were complicated by influences from adjacent cracks.

(2) Based on extrapolated data obtained with the present probe, the minimum detectable crack size (signal to background ratio of approximately two) for tiebolt holes examined in this project is approximately 0.25 mm (10 mils) long by 0.08 mm (3 mils) deep.

(3) Both experimental and theoretical data show that good potential exists to differentiate between small, closely-spaced cracks and single cracks, although more experimental data, theoretical modeling, probe refinements, and signal processing will be required to differentiate between cracks with complex subsurface geometries.

(4) The potential exists to determine crack characterization parameters such as depth, although additional data, modeling, and signal processing will again be required to characterize complex cracks.

(5) The ECP results are readily adaptable to simple imaging processes. A good potential exists for the use of correlation techniques to obtain defect characterization and separation of multiple crack responses.

(6) The signal background is much greater in amplitude than electronic noise and is related to material characteristics.

VI. RECOMMENDATIONS

Based on the results of this project and results obtained from prior investigation of the Electric Current Perturbation method, the following recommendations are made:

(1) Immediate consideration for application to fatigue crack detection in J-79 turbine disk regions such as bores, bolt holes, rabbet areas and dovetail slots.

(2) In the longer term, research and development on the ECP technology should be conducted in support of advanced NDE applicable to retirement for cause on TF-30, F-100 and other advanced engine components.

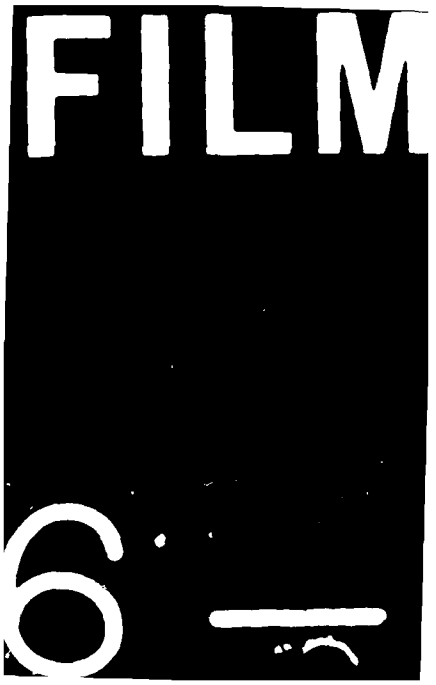
FILM